Geochemistry Geophysics Geosystems G3
AN ELECTRONIC JOURNAL OF THE EARTH SCIENCES
Published by AGU and the Geochemical Society

Article
Volume 9, Number 4
17 April 2008
Q04027, doi:10.1029/2007GC001876
ISSN: 1525-2027

Globally elevated titanium, tantalum, and niobium (TITAN) in ocean island basalts with high $^{3}He/^{4}He$

Matthew G. Jackson
Woods Hole Oceanographic Institution Joint Program, Massachusetts Institute of Technology, 266 Woods Hole Road, Woods Hole, Massachusetts 02543-1525, USA (mjackson@whoi.edu)

Stanley R. Hart
Woods Hole Oceanographic Institution, Mail Stop 22, Woods Hole, Massachusetts 02543-1525, USA

Alberto E. Saal
Department of Geological Sciences, Brown University, 324 Brook Street, Box 1846, Providence, Rhode Island 02912, USA

Nobumichi Shimizu, Mark D. Kurz, and Jerzy S. Blusztajn
Woods Hole Oceanographic Institution, Mail Stop 22, Woods Hole, Massachusetts 02543-1525, USA

Anna C. Skovgaard
Chemical Department, Danish Environmental Protection Agency, DK-1401 Copenhagen, Denmark

[1] We report evidence for a global Ti, Ta, and Nb (TITAN) enriched reservoir sampled by ocean island basalts (OIBs) with high $^{3}He/^{4}He$ ratios, an isotopic signature associated with the deep mantle. Excesses of Ti (and to a lesser degree Nb and Ta) correlate remarkably well with $^{3}He/^{4}He$ in a data set of global OIBs, demonstrating that a major element signature is associated with the high $^{3}He/^{4}He$ mantle. Additionally, we find that OIBs with high $^{3}He/^{4}He$ ratios have moderately radiogenic $^{187}Os/^{188}Os$ (>0.135). The TITAN enrichment and radiogenic $^{187}Os/^{188}Os$ in high $^{3}He/^{4}He$ OIBs indicate that they are melts of a mantle domain that hosts a nonprimitive (nonchondritic) component. The observation of TITAN enrichment in the high $^{3}He/^{4}He$ mantle may be important in balancing the Earth's budget for the TITAN elements. Understanding the origin of the TITAN enrichment is important for constraining the evolution of the enigmatic high $^{3}He/^{4}He$ mantle domain.

Components: 12,074 words, 4 figures, 3 tables.

Keywords: $^{3}He/^{4}He$; FOZO; PHEM; C; OIB; eclogite.

Index Terms: 1025 Geochemistry: Composition of the mantle; 1065 Geochemistry: Major and trace element geochemistry; 1040 Geochemistry: Radiogenic isotope geochemistry.

Received 28 October 2007; **Revised** 16 February 2008; **Accepted** 26 February 2008; **Published** 17 April 2008.

Jackson, M. G., S. R. Hart, A. E. Saal, N. Shimizu, M. D. Kurz, J. S. Blusztajn, and A. C. Skovgaard (2008), Globally elevated titanium, tantalum, and niobium (TITAN) in ocean island basalts with high $^{3}He/^{4}He$, *Geochem. Geophys. Geosyst.*, *9*, Q04027, doi:10.1029/2007GC001876.

1. Introduction

[2] Rare, high $^{3}He/^{4}He$ (>30 Ra, or ratio to atmosphere) ratios measured in lavas erupted at some hot spots, including Hawaii, Iceland, Galapagos and Samoa, are thought to be tracers of buoyantly upwelling mantle plumes that sample an ancient reservoir residing in the mantle [e.g., *Kurz et al.*, 1982; *Hart et al.*, 1992; *Class and Goldstein*, 2005]. The early Earth hosted high $^{3}He/^{4}He$ ratios at least as high as the present-day sun (>100 Ra), and the survival of this primeval isotopic signature in the mantle has important implications for mantle convection and evolution [*Jackson et al.*, 2007b]. High $^{3}He/^{4}He$ ratios in ocean island basalts (OIBs) have been used as evidence that a primitive, undegassed reservoir resides in the Earth's mantle [*Kurz et al.*, 1982; *Allègre et al.*, 1983; *Farley et al.*, 1992]. Variously called FOZO (Focus Zone) [*Hart et al.*, 1992], PHEM (Primitive Helium Mantle) [*Farley et al.*, 1992] or C (Common) [*Hanan and Graham*, 1996], the mantle reservoir hosting high $^{3}He/^{4}He$ is poorly understood. Its precise location (shallow or deep mantle [e.g., *Anderson*, 1998]) and composition are not well known.

[3] Nonetheless, there is a growing consensus that this reservoir hosts a significant component of mantle peridotite, a lithology that may preserve high $^{3}He/^{238}U$, and by inference high $^{3}He/^{4}He$, over time [e.g., *Hart et al.*, 1992; *Anderson*, 1998; *Parman et al.*, 2005; *Heber et al.*, 2007]. Recent work also suggests that the high $^{3}He/^{4}He$ mantle sampled by OIBs may also host a component of recycled eclogite [*Dixon et al.*, 2002; *Brandon et al.*, 2007]. *Albarede and Kaneoka* [2007] even suggest that the high $^{3}He/^{4}He$ mantle domain sampled by OIBs is composed of a U and Th-depleted, high $^{3}He/^{4}He$ pyroxenite. An eclogitic or pyroxenitic component in the high $^{3}He/^{4}He$ reservoir would be evidence that it is not purely primitive. Therefore, understanding the composition of the high $^{3}He/^{4}He$ mantle reservoir is important in formulating models for its origin and long-term survival in the convecting mantle.

[4] Here we identify a remarkable enrichment in the elements Ti, Ta and Nb (TITAN) in high $^{3}He/^{4}He$ lavas from Hawaii, Iceland, Samoa and Galapagos, and show that high $^{3}He/^{4}He$ lavas exhibit moderately radiogenic $^{187}Os/^{188}Os$ ratios (>0.135) that are greater than DMM (depleted MORB mantle, 0.120–0.125 [*Standish et al.*, 2002]) and primitive mantle (0.129 [*Meisel et al.*, 2001]). This unusual combination of geochemical signatures provides an important constraint on the composition and origin of the high $^{3}He/^{4}He$ reservoir sampled by OIBs. The TITAN enrichment and radiogenic $^{187}Os/^{188}Os$ is consistent with the high $^{3}He/^{4}He$ mantle domain hosting a component of recycled, refractory eclogite. However, the TITAN enrichment could also be a product of trace element partitioning between lower mantle phases, such as Ca-perovskite.

2. New Data and Observations

[5] We report new trace element data by ICP-MS (inductively coupled plasma mass spectrometer) on the highest $^{3}He/^{4}He$ lavas from Hawaii (32.3 Ra [*Kurz et al.*, 1982]), Iceland (37.7 Ra [*Hilton et al.*, 1999]) and Samoa (33.8 Ra [*Jackson et al.*, 2007b]) (see Table 1). We also present new $^{3}He/^{4}He$, $^{187}Os/^{188}Os$ and major and trace element data on Samoan and Icelandic lavas with intermediate $^{3}He/^{4}He$ ratios (8–30 Ra) (see Table 2). In Figure 1, these new data are presented together with previously published ICP-MS trace element data for the highest $^{3}He/^{4}He$ Galapagos lava (30.3 Ra [*Kurz and Geist*, 1999; *Saal et al.*, 2007]). These high $^{3}He/^{4}He$ lavas exhibit Ti, Ta, and Nb excesses, or positive anomalies, relative to elements of similar compatibility in peridotite (on a primitive mantle normalized basis). While the association of positive TITAN anomalies and high $^{3}He/^{4}He$ (or plume) signatures was previously observed regionally in Hawaii [*Hauri*, 1996; *Dixon et al.*, 2002], Iceland [*Fitton et al.*, 1997] and the Galapagos [*Kurz and Geist*, 1999; *Saal et al.*, 2007], we suggest that the large, positive TITAN anomalies are a global phenomenon in high $^{3}He/^{4}He$ OIBs. The primitive-mantle normalized trace element patterns (spidergrams) of the highest $^{3}He/^{4}He$ lavas from Hawaii, Iceland, Galapagos and Samoa all share prominent, anomalous enrichment in the TITAN elements compared to elements of similar compatibility in peridotite (Figure 1). The Nb/U ratios in the high $^{3}He/^{4}He$ OIB lavas are all higher than the "average" Nb/U value of 47 previously proposed for OIBs and mid-ocean ridge basalts (MORBs) [*Hofmann et al.*, 1986].

[6] By contrast, the mantle end-members [*Zindler and Hart*, 1986] with low $^{3}He/^{4}He$, including HIMU (high "μ," or $^{238}U/^{204}Pb$ [*Graham et al.*, 1992; *Hanyu and Kaneoka*, 1997]), EM1 (enriched mantle 1) [*Honda and Woodhead*, 2005], EM2 (enriched mantle 2) [*Farley et al.*, 1992; *Workman et al.*, 2004; *Jackson et al.*, 2007a] and DMM

exhibit spidergrams [*Hart and Gaetani*, 2006] that lack such pronounced TITAN anomalies (Figure 1). While HIMU basalts can have positive Nb and Ta anomalies [*Weaver et al.*, 1987; *Weaver*, 1991; *Chauvel et al.*, 1992], they generally have lower anomalies than high $^{3}He/^{4}He$ lavas, and can even have negative Nb anomalies [*Sun and McDonough*, 1989]. Importantly, HIMU lavas exhibit flat or negative Ti-anomalies [*McDonough*, 1991], and thus lack the positive Ti-anomalies observed in high $^{3}He/^{4}He$ lavas.

[7] Available data also indicate that the TITAN enrichment, and radiogenic $^{187}Os/^{188}Os$ signatures, are enhanced with increasing $^{3}He/^{4}He$ in OIB lavas (Figure 2): Large, positive Ti (high Ti/Ti*), Nb (elevated Nb/Nb*) and Ta (Ta/Ta*, not shown) anomalies and moderately radiogenic $^{187}Os/^{188}Os$ (>0.135) are observed in the highest $^{3}He/^{4}He$ basalts (see Figure 2 caption for the formulation of TITAN anomalies). While all high $^{3}He/^{4}He$ lavas (>30 Ra) have large, positive TITAN anomalies and moderately radiogenic $^{187}Os/^{188}Os$, not all lavas with positive TITAN anomalies and radiogenic $^{187}Os/^{188}Os$ have high $^{3}He/^{4}He$. In the plots of TITAN anomalies versus $^{3}He/^{4}He$ and $^{187}Os/^{188}Os$ versus $^{3}He/^{4}He$, the OIB data outline a "wedge-shaped" pattern. For example, Cape Verde lavas have large positive Nb/Nb* values and moderately radiogenic $^{187}Os/^{188}Os$, but they have low $^{3}He/^{4}He$ (Figure 2). Additionally, high $^{3}He/^{4}He$ lavas with negative TITAN anomalies and unradiogenic $^{187}Os/^{188}Os$ are absent in the available data set.

Table 1. Major and Trace Element and Isotopic Composition of the Highest $^{3}He/^{4}He$ Lavas From Four Hot Spots[a]

Hot Spot	Iceland	Samoa	Hawaii	Galapagos
Volcano	Selardalur	Ofu	Loihi	Fernandina
Sample	SEL 97	OFU-04-06	KK18-8	NSK 97-214
Rock Type	Tholeiite	Alkali basalt	Tholeiite	Tholeiite
SiO_2	47.09	***44.84***	48.43	49.44
Al_2O_3	9.96	***11.04***	12.62	14.77
TiO_2	1.22	***4.95***	2.88	3.12
FeOT	10.63	***12.78***	11.90	11.30
MnO	0.15	***0.18***	0.18	0.19
CaO	10.40	***12.42***	12.82	11.60
MgO	19.21	***9.81***	8.06	6.41
K_2O	0.05	***1.14***	0.50	0.39
Na_2O	1.21	***2.24***	2.34	2.46
P_2O_5	0.062	***0.587***	0.265	0.315
$^{87}Sr/^{86}Sr$	0.703465	0.704584	0.703680	0.703290
$^{143}Nd/^{144}Nd$	0.512969	0.512827	0.512945	0.512937
$^{206}Pb/^{204}Pb$	18.653	19.189	18.448	19.080
$^{207}Pb/^{204}Pb$	15.473	15.571	15.447	15.537
$^{208}Pb/^{204}Pb$	38.453	39.202	38.189	38.710
$^{3}He/^{4}He$	37.7	33.8	32.3	30.3
Ni	759	***201***	80	49
Cr	1730	***533***	384	155
V	203	***364***	350	366
Ga		***21***		26
Cu		***80***		83
Zn		***132***		110
Cs	***0.02***	***0.33***	***0.09***	0.07
Rb	***0.92***	***25.6***	***9.12***	7.60
Ba	***19***	***249***	***123***	89
Th	***0.38***	4.0	***0.99***	1.3
U	***0.072***	***0.99***	***0.28***	0.38
Nb	***6.50***	***50.6***	***16.3***	20.0
Ta	***0.43***	***3.84***		1.50
La	***3.85***	***37.9***	***13.8***	14.1
Ce	***8.52***	***80.5***	***32.9***	32.3
Pb	***0.38***	***2.6***	***1.2***	0.93
Pr	***1.23***	***9.99***	***4.62***	4.23
Nd	***5.80***	***44.1***	***20.7***	19.5
Sr	***173***	599	***349***	351
Zr	***56.8***	***293***	***125***	155
Hf	***1.65***	***7.56***	***3.48***	4.15
Sm	***1.78***	***10.8***	***5.33***	5.77
Eu	***0.79***	***3.39***	***1.83***	2.04
Gd	***2.05***	***9.93***	***5.50***	6.01
Tb	***0.35***	***1.40***	***0.87***	1.03
Dy	***2.16***	***7.34***	***4.89***	6.08
Ho	***0.42***	***1.23***	***0.92***	1.21
Y	***10.0***	***30.3***	***21.9***	30.1
Er	***1.06***	***2.70***	***2.24***	3.04
Tm	***0.15***	***0.32***	***0.29***	0.41
Yb	***0.88***	***1.66***	***1.69***	2.46
Lu	***0.13***	***0.23***	***0.24***	0.36
Sc	***33.9***	***31.2***	***35.4***	44.3

Notes to Table 1:

[a] Data in bold italics are reported here for the first time. All other data have been published elsewhere. Trace element data (excluding Ni, Cr, V, Ga, Cu, Zn, and Sc) are by ICP-MS and are here reported for the first time on the high $^{3}He/^{4}He$ samples from Hawaii, Iceland, and Samoa (however, Th and Sr concentrations for the Samoan lava were reported by *Jackson et al.* [2007b]); the trace element data on the Galapagos sample are reported elsewhere [*Saal et al.*, 2007]. The isotope data for all four lavas are also reported elsewhere [*Hilton et al.*, 1999; *Jackson et al.*, 2007b; *Saal et al.*, 2007; *Kurz et al.*, 1983; *Staudigel et al.*, 1984]. Major element data for the Samoan lava are reported here for the first time; major element data for the Hawaii, Iceland, and Galapagos samples are available elsewhere [*Hilton et al.*, 1999; *Saal et al.*, 2007; *Frey and Clague*, 1983]. Samoan major element (and Ni, Cr, V, Ga, Cu, Zn and Sc) data reported here were measured by XRF. Major and trace element data reported here were analyzed on unleached whole rock powders at the Geoanalytical Laboratory at Washington State University. Internal and (estimated) external precision for the major and trace element analyses are given by *Jackson et al.* [2007a]: errors for major elements are 0.11–0.33% (1σ) of the amount present (SiO_2, Al_2O_3, TiO_2, P_2O_5) and 0.38–0.71% (for all other major elements); for the elements measured by ICP-MS, the reproducibility is 0.77–3.2% (1σ) for all elements except for U (9.5%) and Th (9.3%). The Loihi sample was powdered in Tungsten-carbide, and Ta is therefore not reported for this sample. The Nb concentrations for this sample are similar to measurements previously made on Loihi basalts, as are the Nb/La ratios. We consider the Nb data to be of good quality. Major elements are renormalized to 100% totals on a volatile-free basis.

Table 2. New and Published $^{187}Os/^{188}Os$, $^{3}He/^{4}He$, and Major and Trace Element Data for Icelandic and Samoan Lavas[a]

Hot Spot	Sample ID	Lava Flow	Zone[b]	Refs.[c]	TiO_2, wt. %	Th, ppm	Nb, ppm	Ta, ppm	La, ppm	Sm, ppm	Tb, ppm	Os, ppt	$^{187}Os/^{188}Os$	Error (2 σ) in Run Prec.	$^{187}Os/^{188}Os$ Method	$^{3}He/^{4}He$	Error (1 σ) in Run Prec.
Iceland[d]	OS 207901	Haleyarbunga (D2)	WRZ	1,2	0.29	0.024	0.52	0.052	0.569	0.968	0.311	255.1	0.1326	0.0003	FF	10.83	0.60
Iceland	408672	Lágafell	WRZ	1,2	0.29	0.014	0.34	0.044	0.320	0.557	0.169	596.4	0.1344	0.0002	FF	14.09	0.14
Iceland	OS 208222	Vatnsheidi (D8)	WRZ	1,2	0.51	0.066	1.38	0.10	1.11	1.04	0.31	237.5	0.1284	0.0006	FF	11.65	0.22
Iceland	408640	Höfudhreidharmuli	NRZ	1,2	0.82	0.065	1.47	0.10	1.37	1.64	0.46	85.9	0.1342	0.0003	FF	9.75	0.04
Iceland	408647	Langaviti	NRZ	1,2	0.60	0.058	1.04	0.08	1.08	1.19	0.34	55.1	0.1313	0.0006	FF,CT	7.99	0.13
Iceland	408647 rep	Langaviti	NRZ	1									0.1316	0.0004	FF,CT		
Iceland	408643	Arnahvammurhraun	NRZ	1,2	0.77	0.036	0.62	0.050	1.00	1.51	0.45	263.2	0.1360	0.0002	FF	8.92	0.90
Iceland	408634	Theistareykir picrite	NRZ	1,2	0.38	0.023	0.46	0.043	0.47	0.80	0.26	443.7	0.1341	0.0003	FF	8.16	0.43
Iceland	408635	Theistareykir picrite	NRZ	1,2	0.36	0.015	0.35	0.034	0.36	0.71	0.23	1954.9	0.1269	0.0006	FF	9.47	0.10
Iceland	OS 208224	Asar syd (D27)	WRZ	1	0.54	0.039	0.70	0.058	0.63	1.07	0.35	281.8	0.1361	0.0003	FF	***8.2***	***1.0***
Iceland	OS 208224 rep	Asar syd (D27)rep	WRZ	1								255.2	0.1360	0.0008			
Iceland	OS 208225	Dimmidalur (D29)	WRZ	1	0.58	0.053	0.87	0.07	0.79	1.20	0.38	120.2	0.1307	0.0005	FF	***23.5***	***4.5***
Iceland	SK 82-06	SW of Blagnipa	WRZ	3	0.89	***0.111***	***2.13***	***0.15***	***1.78***	***1.66***	***0.45***	***240.8***	***0.1301***	***0.0006***	***FF***	20.0	
Iceland	SK 82-13	Thrihyrningur	ERZ	3	2.79	***1.15***	***21.6***	***1.34***	***14.8***	***5.41***	***0.84***	***27.2***	***0.1288***	***0.0024***	***FF***	26.2	
Iceland	SK 82-27	Sigalda	ERZ	3	1.73	***0.54***	***8.83***	***0.58***	***6.56***	***3.54***	***0.74***	***29.8***	***0.1274***	***0.0008***	***FF***	20.8	
Iceland	408702	Kambsfell	WRZ	2	***0.89***	***0.156***	***2.58***	***0.18***	***1.97***	***1.75***	***0.48***	***51.2***	***0.1363***	***0.0011***	***FF***	20.4	0.08
Iceland	408709	Kistufell	NRZ	2,4	0.90	0.172	3.50	0.25	2.43	1.82	0.46	***225.9***	***0.1315***	***0.0008***	***FF***	15.65	0.07
Iceland	408712	Kistufell	NRZ	2,4	1.02	0.164	3.56	0.24	2.50	1.96	0.48	***208.1***	***0.1329***	***0.0004***	***FF***	16.79	0.09
Iceland	408730	Bláfell	NRZ	2	***0.70***	***0.070***	***2.24***	***0.15***	***1.78***	***1.40***	***0.41***	***195.0***	***0.1293***	***0.0007***	***FF***	10.54	0.04
Iceland	408713	Dyngjufjell Ytri	NRZ	2	***1.38***	***0.447***	***7.06***	***0.46***	***5.40***	***3.14***	***0.67***					19.58	0.09
Iceland	SK 82-12	Kalfstindar	WRZ	3	1.37							***168.3***	***0.1303***	***0.0008***	***FF***	13.8	
Iceland	SK 82-01B	West Jarlhettur	WRZ	3	1.91							***133.1***	***0.1307***	***0.0009***	***FF***	15.9	
Iceland	HS-806	Eiriksjökull	WRZ	3,5	1.02							97.7	0.1385	0.0030	FF	8.7	
Iceland	IC-117	Dvergalda	WRZ	3,5	0.82							295.9	0.1337	0.0013	FF	21.6	
Samoa[e]	OFU-04-06			6	***4.95***	3.96	***50.6***	***3.84***	***37.9***	***10.8***	***1.40***	***105.6***	***0.1335***	***0.0013***	***FF***	33.8	0.2
Samoa	OFU-04-03			6	***3.83***	3.26	***36.9***	***2.87***	***29.6***	***8.45***	***1.13***	***104.4***	***0.1320***	***0.0005***	***FF***	24.0	0.1
Samoa	OFU-04-09			6	***5.36***	3.25	***40.2***	***3.09***	***32.8***	***9.56***	***1.31***					25.6	0.5
Samoa	OFU-04-14			6	***3.55***	1.95	***22.8***	***1.77***	***18.6***	***6.05***	***0.86***					25.0	0.2
Samoa	OFU-04-05			6	***4.96***	4.24	***48.7***	***3.77***	***38.5***	***10.8***	***1.44***					24.4	0.1
Samoa	OFU-04-08			6	***5.42***	4.06	***49.4***	***3.78***	***38.1***	***11.0***	***1.47***					21.3	0.3

Table 2. (continued)

Hot Spot	Sample ID	Lava Flow	Zone[b]	Refs.[c]	TiO_2, wt. %	Th, ppm	Nb, ppm	Ta, ppm	La, ppm	Sm, ppm	Tb, ppm	Os, ppt	$^{187}Os/^{188}Os$	Error (2σ) in Run Prec.	$^{187}Os/^{188}Os$ Method	$^{3}He/^{4}He$	Error (1σ) in Run Prec.
Samoa	OFU-04-15			6	***4.88***	3.89	***48.4***	***3.63***	***34.6***	***9.70***	***1.30***					29.6	0.2
Samoa	OFU-04-12			6	***3.89***	3.29	***34.4***	***2.63***	***33.7***	***8.78***	***1.24***					21.2	0.3
Samoa	OFU-04-16			6	***5.35***	3.54	***44.7***	***3.40***	***31.4***	***9.02***	***1.28***					19	1
Samoa	OFU-04-10			6	***4.31***	3.65	***41.6***	***3.40***	***32.9***	***9.34***	***1.27***					22.0	0.2

[a] New data presented in this paper are in bold italics. Errors are reported in Table 2 as standard error of the mean. FF, fusion flux; CT, carius tube.
[b] The different regions in Iceland are reported as NRZ (Northern Rift Zone), WRZ (Western Rift Zone), and ERZ (Eastern Rift Zone).
[c] Published data can be found for the following references: 1, *Skovgaard et al.* [2001]; 2, *Breddam et al.* [2000]; 3, *Kurz et al.* [1985]; 4, *Breddam* [2002]; 5, *Martin* [1991]; 6, *Jackson et al.* [2007b].
[d] Iceland data: Unpublished helium isotope data on the Icelandic samples are after the same method reported by *Breddam et al.* [2000]. New $^{187}Os/^{188}Os$ major and trace element data on the Icelandic samples are after the same method as reported by *Skovgaard et al.* [2001]. The $^{187}Os/^{188}Os$ measurements reported here were made following Os preconcentration using a nickel sulfide fire assay technique. The $^{187}Os/^{188}Os$ isotope ratios were measured by negative thermal ionization mass spectrometry as single multiplier analyses at WHOI. Total blanks were less than 0.7 pg. Major and trace element data were obtained on samples powdered in a SPEX corundum shaker mill. Major elements were measured by XRF on fused glass disks at the Geological Survey of Denmark and Greenland. Errors are between 0.25 and 4% (2 S.D.) for major elements. Trace element measurements on the Icelandic rocks were made by ICPMS at the University of Durham, U.K. On the basis of replicate analyses of samples and an in-house standard, the analytical precision (1 S.D.) is <5% for all reported trace elements, except Nb (10%).
[e] Samoa data: New major and trace element analyses on the Samoan lavas were made on unleached whole-rock powders at the Washington State University Geoanalytical Laboratory using the same method as reported in Table 1. The $^{187}Os/^{188}Os$ isotope analyses were made at WHOI following the same protocol as reported by *Workman et al.* [2004]. Following a flux fusion technique for concentrating Os, $^{187}Os/^{188}Os$ was measured by sparging OsO_4 into a Finnigan Element Magnetic Sector ICP-MS. Blank corrections were similar to those of *Workman et al.* [2004].

[8] The TITAN anomalies in high $^{3}He/^{4}He$ lavas reflect their mantle sources, and do not appear to be a result of shallow (<200 km) mantle melting or crystal fractionation processes. While *Kelemen et al.* [1993] suggested that melts in the garnet stability field can produce positive Ti-anomalies, we do not find that indicators of melting in the garnet stability field (such as steeply sloping primitive mantle-normalized rare earth patterns) correlate with Ti/Ti* in the lavas compiled in Figure 2. Even if melting in the garnet stability field were responsible for the Ti-anomalies in some high $^{3}He/^{4}He$ lavas, available partition coefficients indicate that such a melting process could not generate the positive Nb and Ta anomalies in the same lavas. Crystal fractionation is also unlikely to be responsible for the positive TITAN anomalies in the high $^{3}He/^{4}He$ OIBs, as indicators of magma evolution (like MgO content) exhibit no relationship with the magnitude of the anomalies. As a precaution, lavas that have suffered high degrees of crystal fractionation and have MgO < 5.3 wt.% have been excluded from the top two panels of Figure 2.

3. Case for a Refractory, Rutile-Bearing Eclogite Component in the High $^{3}He/^{4}He$ Mantle Sampled by OIBs

3.1. TITAN Enrichment and High $^{187}Os/^{188}Os$: Evidence for Refractory Eclogite

[9] The lack of large TITAN anomalies in DMM (Figure 1) demonstrates that phases contained in upper mantle peridotites do not preferentially sequester the TITAN elements relative to other incompatible lithophile elements. By contrast, subduction zone lavas are TITAN-depleted, indicating that processes operating in their mantle sources can fractionate TITAN from the other lithophile trace elements. It was suggested that eclogite melting, which may have occurred in some subduction zones (especially in the subduction zones of an early, hot Earth), may have generate rutile-bearing residues that are residually enriched in TITAN elements [e.g., *McDonough*, 1991]. Experimental studies indicate that the TITAN elements are strongly partitioned into rutile during eclogite melting [*Green and Pearson*, 1986; *Ryerson and Watson*, 1987; *Ayers*, 1998; *Stalder et al.*, 1998; *Foley et al.*, 2000; *Schmidt et al.*, 2004; *Kessel et al.*, 2005], thereby generating positive TITAN anomalies in refractory, rutile-bearing slab residues.

Available parititioning data therefore suggest that the presence of eclogite is a viable explanation for the TITAN anomalies.

[10] Like TITAN-enrichment, radiogenic $^{187}Os/^{188}Os$ is not a geochemical signature typically associated with a peridotite reservoir. While peridotites tend to have low Re/Os and $^{187}Os/^{188}Os$, mafic igneous rocks generally exhibit elevated Re/Os and $^{187}Os/^{188}Os$ ratios [*Walker et al.*, 1989; *Reisberg et al.*, 1991, 1993; *Hauri and Hart*, 1993; *Snow and Reisberg*, 1995; *Becker*, 2000]. Oceanic crust enters subduction zones with initially high Re/Os, and owing to moderate compatibility of Re in garnet, oceanic crust may retain high Re/Os (and with time, radiogenic $^{187}Os/^{188}Os$) ratios during subduction zone processing in the garnet stability field [*Righter and Hauri*, 1998]. While it has been suggested that Os and Re are extracted from the slab in the subduction zone [e.g., *Brandon et al.*, 1996; *McInnes et al.*, 1999; *Becker et al.*, 2000], we note that the Re/Os ratios of altered oceanic crust ($^{187}Re/^{188}Os$ averages of 349 and 353 in composites of two separate drill cores [*Peucker-Ehrenbrink et al.*, 2003]) and oceanic crust gabbros ($^{187}Re/^{188}Os$ average of 472 [*Hart et al.*, 1999]) are similar to the ratios found in metabasalts metamorphosed in paleosubduction zones (median $^{187}Re/^{188}Os$ = 326, including eclogites, blueschists and mafic granulites [*Becker*, 2000]). Thus, there is ample evidence that high Re/Os ratios can be preserved in the slab during subduction zone metamorphism. The observation of moderately radiogenic $^{187}Os/^{188}Os$ in high $^{3}He/^{4}He$ lavas is consistent with a refractory eclogite component in their mantle sources.

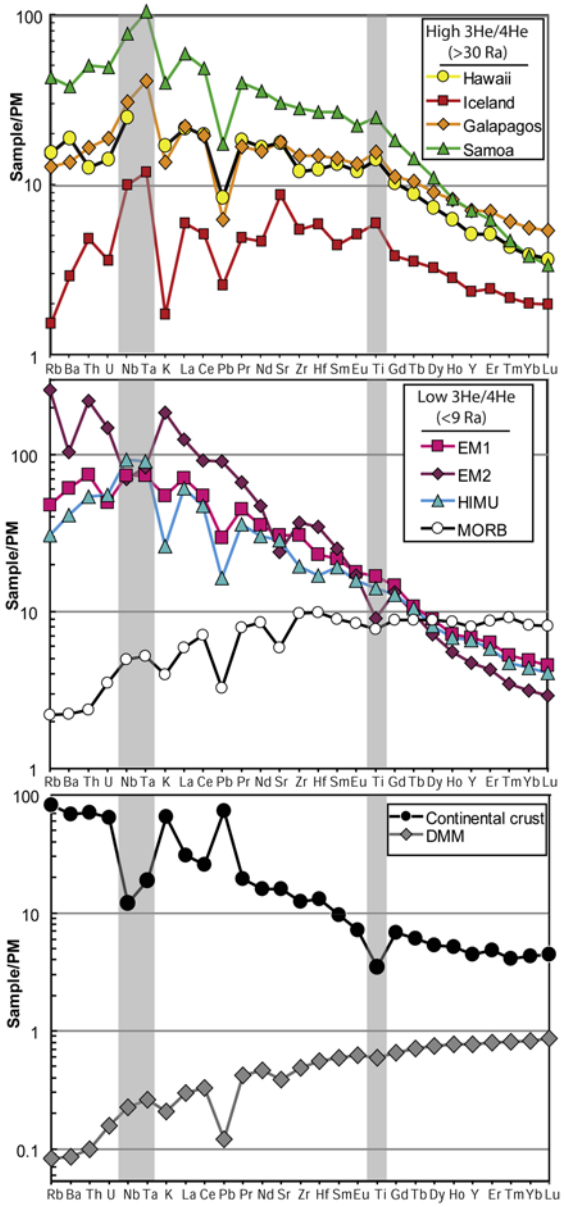

Figure 1. Titanium, tantalum, and niobium (TITAN) are highly enriched in ocean island basalts (OIBs) with high $^{3}He/^{4}He$. (top) Primitive mantle (PM) normalized trace element data (spidergrams) for basalts with the highest $^{3}He/^{4}He$ (>30 Ra) from 4 different hot spots. All high $^{3}He/^{4}He$ samples exhibit TITAN enrichment relative to neighboring elements on the spidergrams. (middle) Spidergrams for the low $^{3}He/^{4}He$ (<9 Ra) mantle end-members. EM1 lavas are from Pitcairn, EM2 lavas are from Samoa, and HIMU lavas are from Mangaia and Tubuaii. Spidergrams for the mantle end-members and MORB are from *Hart and Gaetani* [2006] and (for EM2) *Jackson et al.* [2007a]. TITAN enrichment is not as pronounced, or is absent, in the average spidergrams of the low $^{3}He/^{4}He$ mantle end-members. (bottom) Spidergrams for DMM [*Workman and Hart*, 2005] and continental crust [*Rudnick and Gao*, 2003] indicate that these two shallow earth reservoirs are not entirely geochemically complementary: TITAN depletion in the continents is not balanced by corresponding enrichment in DMM. However, the TITAN-enrichment in high $^{3}He/^{4}He$ lavas suggests that these lavas sample a (deeper) mantle reservoir that hosts part of the TITAN that is missing in the shallow geochemical reservoirs, DMM, and continental crust. Sources of the $^{3}He/^{4}He$ data for the mantle end-members and the high $^{3}He/^{4}He$ lavas can be found in the text and in Table 1.

3.2. TITAN Enrichment With Concomitant Depletion in the ^{4}He-Producing Elements, U and Th

[11] While recycled oceanic crust has been suggested to be ubiquitous in the mantle sources

beneath hot spots [*Sobolev et al.*, 2007], the close association of a refractory, TITAN-enriched mafic component with the high $^{3}He/^{4}He$ mantle may appear contradictory since eclogites are quantitatively degassed in subduction zones [*Staudacher and Allègre*, 1988; *Moreira and Kurz*, 2001; *Moreira et al.*, 2003]. Far from hosting the high $^{3}He/^{4}He$ signature in the mantle source of high

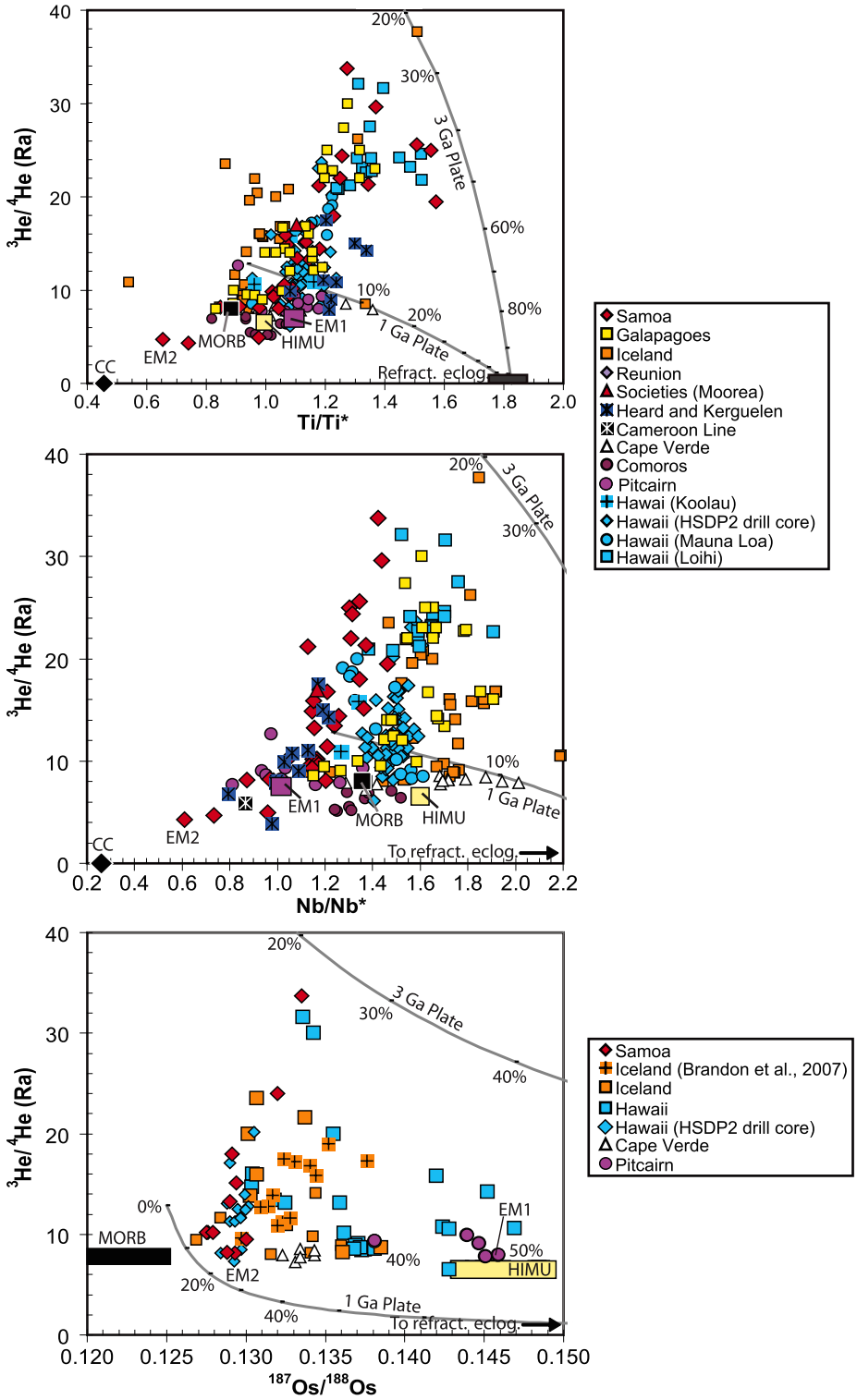

Figure 2

$^3He/^4He$ OIB lavas, the eclogite will instead contribute ^4He (via alpha decay of U and Th) and generate low time-integrated $^3He/^4He$ ratios. However, the long-term ^4He production of an eclogite can be greatly reduced by melt (or fluid) extraction of highly incompatible elements like U and Th from the slab during subduction processing. By contrast, the TITAN elements will be conserved if melt (or fluid) extraction occurs in the presence of rutile [e.g., *McDonough*, 1991]. In fact, the positive TITAN anomaly is formed by relative enrichment of TITAN due to conservation of Ti, Ta and Nb and concomitant loss of incompatible elements like U and Th. Therefore, the TITAN-enriched, U and Th-poor refractory eclogite composition proposed by *McDonough* [1991] will not produce significant post-subduction radiogenic ^4He ingrowth.

3.3. Refractory Eclogite and High $^3He/^4He$ Peridotite: The Raw Materials for the High $^3He/^4He$ OIB Mantle

[12] While refractory, rutile-bearing eclogite possesses positive TITAN anomalies, it is unlikely to have intrinsically high $^3He/^4He$ ratios: high $^3He/^4He$ signatures in the TITAN-enriched, high $^3He/^4He$ OIB source must be derived from another lithology. Ancient mantle peridotites can potentially preserve elevated $^3He/^4He$ ratios over time [*Hart et al.*, 1992; *Anderson*, 1998; *Parman et al.*, 2005; *Heber et al.*, 2007; *Jackson et al.*, 2007b] if they were isolated from the convecting mantle early in Earth's history. However, mantle peridotites do not generally exhibit positive TITAN anomalies [*McDonough*, 1991]. Alone, neither eclogite nor peridotite can contribute both TITAN-enrichment and high $^3He/^4He$ to the mantle source sampled by high $^3He/^4He$ OIB lavas. Both refractory eclogite and the high $^3He/^4He$ peridotite are required to generate such a mantle source. Thus, an important question is how the TITAN-enriched eclogites came to be associated (i.e., mixed) with high $^3He/^4He$ peridotites in the mantle.

3.4. Peridotite and Eclogite Portions of Ancient Subducted Slabs: A High $^3He/^4He$, TITAN-Enriched "Package"

[13] One possible explanation for the generation of a hybrid lithology in the high $^3He/^4He$ OIB mantle is that the crust and mantle components of ancient (>2 Ga), subducted oceanic lithosphere contain the raw materials required for the generation of a mantle source sampled by high $^3He/^4He$ basalts. TITAN-enriched, degassed, refractory eclogite

Figure 2. Relationships between TITAN anomalies, $^{187}Os/^{188}Os$, and $^3He/^4He$ in representative hot spot lavas. High $^3He/^4He$ lavas all have elevated (top) Ti/Ti*, (middle) Nb/Nb*, and (bottom) $^{187}Os/^{188}Os$. With increasing positive TITAN anomalies and $^{187}Os/^{188}Os$ ratios in the OIBs, the maximum observed $^3He/^4He$ increases. All samples with high $^3He/^4He$ (>20 Ra) host radiogenic $^{187}Os/^{188}Os$ (>0.130). The model curves are not meant to describe the global OIB array. Instead, the model curves are intended to constrain the mixing proportions of eclogite and peridotite in the high $^3He/^4He$ mantle sampled by the highest $^3He/^4He$ lavas (>30 Ra). Mixing is marked at 10% intervals, with increasing contribution from eclogite. The 3 Ga model curve describes mixing between the high $^3He/^4He$ (low TITAN anomaly) peridotitic and low $^3He/^4He$ (high TITAN anomaly) refractory eclogitic portions of an ancient oceanic plate. More contribution from eclogite tends to generate lower $^3He/^4He$ ratios in the peridotite-eclogite mixture over time, and 20–25% eclogite added to 75–80% peridotite generates the $^{187}Os/^{188}Os$, Ti, and Nb anomalies in the highest $^3He/^4He$ lavas. The 1 Ga model curve describes mixing between the peridotitic and eclogitic portions of a more recently subducted oceanic plate and demonstrates that younger plates do not generate sufficiently high $^3He/^4He$ in the model. The most extreme lava in Figure 2 (sample SEL 97) is the highest $^3He/^4He$ lava available that also has a complete suite of trace elements measured by ICP. Unfortunately, $^{187}Os/^{188}Os$ is not available for this sample, and the $^{187}Os/^{188}Os$ of the highest $^3He/^4He$ mantle is instead approximated using lavas (with $^3He/^4He$ > 30 Ra) from Hawaii and Samoa. Samoan posterosional (from Savai'i) data are excluded; all $^{187}Os/^{188}Os$ data in Figure 2 are > 50 ppt Os, except Cape Verde (>10 ppt) and Pitcairn (>20 ppt). The $^3He/^4He$, $^{187}Os/^{188}Os$, and trace element data for representative OIB samples are from the GEOROC database (http://georoc.mpch-mainz.gwdg.de/) and from the helium database of *Abedini et al.* [2006]. The $^3He/^4He$ data from OIBs are not filtered on the basis of helium concentrations. However, samples suggested to have suffered shallow contamination by crust (e.g., several samples in the work of *Macpherson et al.* [2005]) were not included. Additionally, very evolved rocks (MgO < 5.3 wt.%) were excluded from the top two panels, so as to preclude the effects of extensive fractional crystallization on the various trace element ratios (e.g., Ti/Ti* and Nb/Nb*). Using Ba/Rb as a filter for alteration, samples with high ratios (Ba/Rb > 25) were not considered. Only trace element (Th, La, Sm, Tb) data measured by ICP-MS and neutron activation are included, thereby eliminating samples with low-precision trace element measurements. $Nb/Nb^* = Nb_N/(Th_N \times La_N)^{0.5}$, $Ta/Ta^* = Ta_N/(Th_N \times La_N)^{0.5}$, and $Ti/Ti^* = Ti_N/(Sm_N \times Tb_N)^{0.5}$, where N means normalized to primitive mantle.

exists at the top of downgoing slabs. By contrast, the lowermost portion of the downgoing plate is composed of ancient, high $^{3}He/^{4}He$ peridotite. While near-surface mantle peridotites underlying the oceanic crust degas efficiently during melt extraction at mid-ocean ridges, the lherzolitic peridotite in the deepest regions of the oceanic mantle lithosphere suffer little melt extraction and remain less degassed. We assume that the deepest portion of the ancient oceanic mantle lithosphere is a viable reservoir for preserving high $^{3}He/^{4}He$ over time.

[14] After processing in subduction zones, the crustal portion of the subducted plate hosts TITAN enrichment, and the peridotite in the deep oceanic mantle lithosphere remains unscathed by subduction zone processes. The two components, TITAN-enriched eclogite and high $^{3}He/^{4}He$ peridotite, could be intimately associated as a "package" in space and time within a subducted plate, a geometry that is conducive to later mixing in the mantle.

[15] We present one possible model for the generation of the high $^{3}He/^{4}He$ mantle sampled by OIBs, whereby the eclogitic and peridotitic components of an oceanic plate are subducted and isolated from the convecting mantle at 3 Ga and mixed during long-term storage in the lower mantle (Figure 3). In this simple model, we assume that the upper mantle began with a primitive composition [*McDonough and Sun*, 1995] at 4.4 Ga, and evolved by continuous depletion to the present-day DMM composition of *Workman and Hart* [2005]. Oceanic plates were continuously injected into the mantle over this time period, and the eclogitic and peridotitic portions of these subducted plates were thoroughly mixed in the lower mantle and were later sampled by upwelling mantle plumes and erupted at hot spots. We assume that neither lithology is preferentially sampled during melting under hot spots, such that low degree melts of the peridotite-eclogite mixture will not preferentially sample the refractory eclogite.

[16] In order to develop a quantitative geochemical model for the $^{3}He/^{4}He$, $^{187}Os/^{188}Os$, and TITAN of the two lithologies (peridotite and eclogite) in a subducted plate, we make the following assumptions about their compositions over time. We note that such models are inherently uncertain due to the large uncertainties in the input parameters. Most notably, the concentrations of the volatile elements such as helium are poorly known in the deep mantle and in the early Earth.

3.4.1. The $^{3}He/^{4}He$ of Ancient Oceanic Mantle Lithosphere and Refractory Eclogite

[17] The $^{3}He/^{4}He$ of DMM is thought to have decreased significantly over time (Figure 3). However, portions of lithospheric peridotite are removed from the upper mantle during subduction of oceanic plates and are not subject to further depletion. In the model presented here, the subducted peridotite from the base of the oceanic lithosphere is assumed to have the same composition as DMM at the time of subduction (the base of the mantle lithosphere has had so little melt extracted during the most recent melting event that its composition is well approximated by the composition of DMM at the time of subduction). The peridotite at the base of the mantle lithosphere "locked in" the high $^{3}He/^{4}He$ and $^{3}He/^{238}U$ ratios of ancient, less-depleted DMM, and evolved by closed-system decay of U and Th. By contrast, if the subducted portion of ancient oceanic mantle lithosphere had remained within the convecting upper mantle, it would have evolved by continuous melt extraction to become modern DMM with low $^{3}He/^{4}He$ and $^{3}He/^{238}U$ (see Figure 3, Table 3, and Appendix A for details of $^{3}He/^{4}He$ evolution in the mantle). Consequently, following subduction and isolation, the $^{3}He/^{4}He$ of the isolated, ancient peridotite from the base of the oceanic lithosphere rapidly diverged from (and preserved higher $^{3}He/^{4}He$ than) its upper mantle counterpart, which continued to be depleted (in He relative to U and Th; see Appendix A) by continental and oceanic crust extraction (Figure 3).

[18] For comparison, the $^{3}He/^{4}He$ evolution of the subducted eclogite is modeled using the trace element composition of a hypothetical refractory eclogite calculated by *McDonough* [1991] (see Figure 4 for a spidergram of the refractory eclogite). The eclogite is assumed to start with a $^{3}He/^{4}He$ ratio equal to DMM at its time of isolation, and following over 99% degassing in the subduction zone, the U and Th of the eclogite continue to generate ^{4}He by decay, thus rapidly diminishing the $^{3}He/^{4}He$ of the eclogite over time (Figure 3 and Table 3). Degassing of the eclogite portion of the subducted slab is simulated by increasing the $^{238}U/^{3}He$ of the eclogite by a factor of 1,000 relative to contemporary DMM.

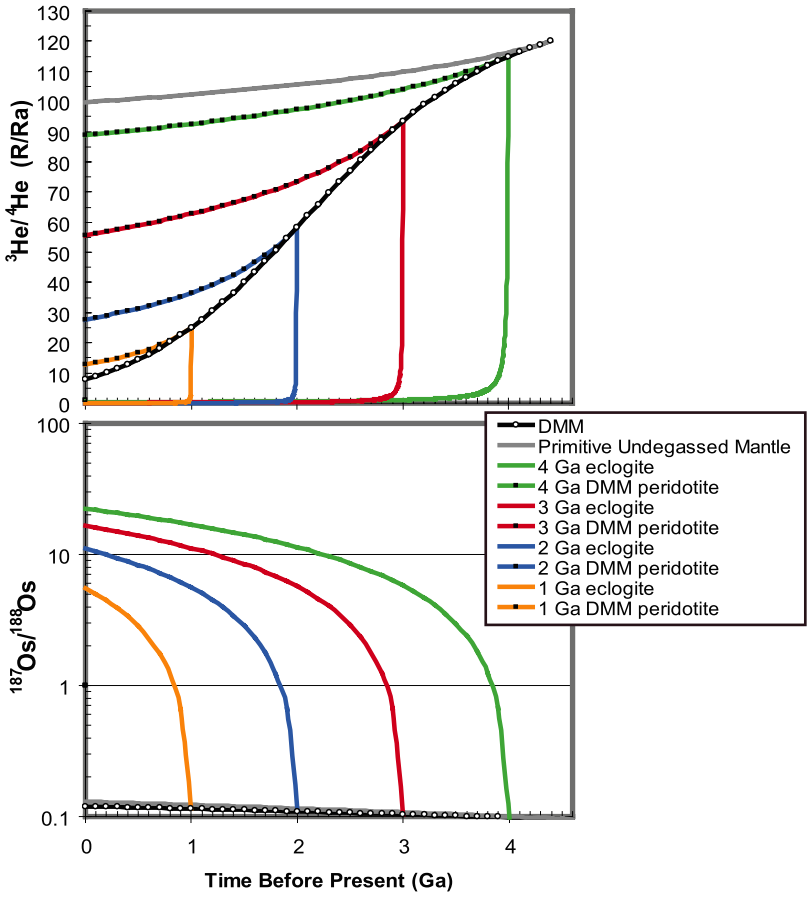

Figure 3. Time evolution of $^3He/^4He$ and $^{187}Os/^{188}Os$ of DMM, ancient subducted lithospheric peridotite, and eclogite. (top) At 4.4 Ga, DMM starts forming by melt extraction from primitive mantle to form continental and oceanic crust, and the $^3He/^4He$ trajectories of DMM and the (hypothetical) primitive undegassed mantle separate immediately. Due to continuous depletion by melt extraction, DMM evolves low $^3He/^4He$. Portions of the ancient lithospheric peridotite, which compose the lowermost portion of downgoing slabs, are sent into the lower mantle throughout geologic time. Model curves are shown at 1 Ga intervals, and this is not intended to imply that the isolation of oceanic plates is episodic. The isolated peridotite portions of the downgoing slabs are modeled as having exactly the same U, Th/U, $^{238}U/^3He$, and $^3He/^4He$ as ambient DMM at the time of isolation, and they preserve higher $^3He/^4He$ than DMM due to their isolation from further melt depletion. Also shown is the concomitant subduction of the eclogitic portions of the same slabs, which begin with the same $^3He/^4He$ as DMM at the time of subduction; the U and Th of the subducted refractory eclogite are from *McDonough* [1991] and are shown in Table 3. To simulate degassing, the $^{238}U/^3He$ of the eclogite is increased by a factor of 1000 relative to the contemporary DMM composition, and as a result the $^3He/^4He$ ratios of the subducted eclogites rapidly decrease. (bottom) The $^{187}Os/^{188}Os$ of Primitive Mantle (0.130 [*Meisel et al.*, 2001]) and DMM (0.125 [*Standish et al.*, 2002]) are very similar. The time evolution of $^{187}Re/^{188}Os$ of ancient subducted peridotite from the base of the oceanic mantle lithosphere is approximated by the trajectory of DMM in Figure 3 (a continuous depletion model is not used to describe the evolution of $^{187}Os/^{188}Os$ of DMM). The present-day $^{187}Re/^{188}Os$ of the refractory eclogite is from *Becker* [2000], and this composition generates increasingly radiogenic present-day $^{187}Os/^{188}Os$ for earlier isolation times. Refer to Appendix A and Table 3 for all parameters used in the model. When 20–25% of a refractory eclogite from an oceanic plate subducted at 3 Ga is mixed together with 75–80% of the peridotitic portion of the same plate, the models generate the $^3He/^4He$ and $^{187}Os/^{188}Os$ of the mantle sampled by the highest $^3He/^4He$ (>30 Ra) OIBs (see Figure 2 for mixing results). Note that the very radiogenic Os of the eclogite is vastly reduced in the mixture due to the low Os contents of the eclogite (6 ppt) and the high Os contents of the isolated DMM peridotite (3,000 ppt).

Table 3. Components Used to Model He, Os, and TITAN Anomalies in the High $^3He/^4He$ Mantle Sampled by OIBs[a]

	$^{238}U/^3He$[b]	^3He, atoms/g[b]	$^3He/^4He$,[c] Ra	^4He, atoms/g	$^{232}Th/^{238}U$	$^{187}Re/^{188}Os$	Os, ppt	$^{187}Os/^{188}Os$	Th, ppm	U, ppm	Nb, ppm	La, ppm	Sr, ppm	Nd, ppm	Zr, ppm	Sm, ppm	Eu, ppm	Ti, ppm	Gd, ppm	Tb, ppm
Undegassed mantle[d]	7.00E+01	7.3E+11	99.6	5.3E+15	4.05	0.396	3400	0.130	0.0795	0.0203	0.658	0.648	19.9	1.25	10.5	0.406	0.154	1205	0.54	0.099
Present-day DMM[e]	5.40E+04	1.5E+08	8.0	1.3E+13	2.55	0.377	3000	0.125	0.0079	0.0032	0.149	0.192	7.664	0.581	5.08	0.239	0.096	716	0.36	0.070
Pure DMM peridotite component[f]																				
DMM peridotite (isolated at 0 Ga, today)	5.40E+04	1.5E+08	8.0	1.3E+13	2.55	0.377	3000	0.125	0.0079	0.0032	0.149	0.192	7.66	0.581	5.08	0.239	0.096	716	0.36	0.070
DMM peridotite (isolated at 1 Ga)	1.19E+04	1.0E+09	12.8	5.8E+13	2.81	0.377	3000	0.125	0.0134	0.0049	0.207	0.253	9.52	0.692	5.99	0.270	0.107	806	0.39	0.076
DMM peridotite (isolated at 2 Ga)	2.63E+03	7.1E+09	27.7	1.8E+14	3.12	0.377	3000	0.125	0.0226	0.0074	0.291	0.334	11.83	0.823	7.07	0.304	0.119	907	0.43	0.082
DMM peridotite (isolated at 3 Ga)	5.80E+02	4.9E+10	55.6	6.3E+14	3.47	0.377	3000	0.125	0.0381	0.0113	0.409	0.440	14.69	0.980	8.34	0.343	0.132	1021	0.48	0.089
DMM peridotite (isolated at 4 Ga)	1.28E+02	3.4E+11	88.6	2.7E+15	3.85	0.377	3000	0.125	0.0644	0.0172	0.574	0.580	18.25	1.166	9.83	0.387	0.148	1149	0.52	0.096
Pure eclogite component[g,h]																				
Refractory eclogite (isolated at 0 Ga, today)	5.40E+07	2.1E+06	8.0	1.9E+11	2.55	325	6	0.125	0.11	0.044	4.5	1.7	63	5.0	50	1.9	0.7	10500	2.7	0.5
Refractory eclogite (isolated at 1 Ga)	1.19E+07	9.4E+06	0.027	2.5E+14	2.55	325	6	5.5	0.11	0.044	4.5	1.7	63	5.0	50	1.9	0.7	10500	2.7	0.5
Refractory eclogite (isolated at 2 Ga)	2.63E+06	4.2E+07	0.057	5.4E+14	2.55	325	6	11.0	0.11	0.044	4.5	1.7	63	5.0	50	1.9	0.7	10500	2.7	0.5
Refractory eclogite (isolated at 3 Ga)	5.80E+05	1.9E+08	0.153	9.1E+14	2.55	325	6	16.6	0.11	0.044	4.5	1.7	63	5.0	50	1.9	0.7	10500	2.7	0.5
Refractory eclogite (isolated at 4 Ga)	1.28E+05	8.7E+08	0.438	1.4E+15	2.55	325	6	22.3	0.11	0.044	4.5	1.7	63	5.0	50	1.9	0.7	10500	2.7	0.5

[a] All values are calculated for the present day. The $^{238}U/^3He$, U, $^{232}Th/^{238}U$, $^3He/^4He$, and trace element budgets of DMM at all times (4 Ga to present) are calculated using the continuous transport equations in Appendix A and initial values provided in Table 3.

[b] The undegassed mantle has been a closed system to all elements, volatile and nonvolatile, since 4.4 Ga. The $^{238}U/^3He$ of undegassed mantle is based on a primitive mantle U concentration [*McDonough and Sun*, 1995] and a ^3He concentration of 7.3×10^{11} atoms/g, a ^3He value that is well within the range suggested for the undegassed mantle in the literature (1.1×10^{11} atoms/g from *Class and Goldstein* [2005] and $\sim 1 \times 10^{12}$ atoms/g in the D″ layer from *Tolstikhin and Hofmann* [2005]). To simulate >99% degassing of the slab in the subduction zone, the $^{238}U/^3He$ value of the refractory eclogite is taken to be a factor of 1,000 times greater than the $^{238}U/^3He$ of DMM peridotite at the time of subduction. The $^3He/^4He$ of the eclogite is assumed to be the same as ambient DMM at the time of subduction.

[c] At 4.4 Ga, the mantle is assumed to have had a $^3He/^4He$ ratio of 120 Ra, a ratio that is similar to the present-day atmosphere of Jupiter [*Niemann et al.*, 1996]; given the assumed $^{238}U/^3He$ and $^{232}Th/^{238}U$ primitive mantle ratios, closed system evolution yields a present-day $^3He/^4He$ ratio of 99.6 Ra (see Appendix A). Using the continuous transport equations in Appendix A, the $^3He/^4He$ ratios of isolated lithospheric peridotite throughout time are the same as ambient upper mantle DMM at the time of subduction and isolation.

[d] The trace element concentrations for undegassed mantle (excluding Os and He) are from *McDonough and Sun* [1995]. The $^{187}Os/^{188}Os$ is from *Meisel et al.* [2001], and the Os and $^{187}Re/^{188}Os$ are from *McDonough and Sun* [1995].

[e] The trace element concentrations (excluding He and Os) for present-day DMM are from *Workman and Hart* [2005]. The $^{187}Os/^{188}Os$ of DMM is from *Standish et al.* [2002].

[f] Using the continuous transport equations in Appendix A, the U and Th contents of the DMM peridotite are calculated to be the same as ambient upper mantle during the time of subduction and isolation; all other trace elements concentrations (except Os) are calculated the same way. Helium concentrations are derived from the calculated $^{238}U/^3He$ and U concentrations.

[g] The $^{187}Re/^{188}Os$ and Os concentrations for refractory eclogite are the median values reported for metamorphosed metabasalts by *Becker* [2000]. The various $^{187}Os/^{188}Os$ values shown for the recycled eclogites are then calculated assuming different isolation times of the same eclogite.

[h] Four of the trace elements for the refractory eclogite (Nb, La, Zr and Ti) were provided explicitly by *McDonough* [1991]. Th, Sr, Nd, Sm, Eu, and Gd were estimated from Figure 5 of the same source. U concentrations for the refractory eclogite are not provided by *McDonough* [1991]. They are estimated using the Th concentration provided and assuming a Th/U ratio of 2.5. The abundance of Tb (used to calculate Ti/Ti*) is not provided by *McDonough* [1991], and its concentration in the refractory eclogite is set by a linear (on a Primitive Mantle normalized basis) extrapolation from Gd and Sm, which are provided. The trace element composition of *McDonough*'s [1991] hypothetical eclogite is quite similar to the eclogites with the highest Nb/Th and Ti/Sm (proxies for Nb and Ti anomalies) in the eclogite data set of *Becker et al.* [2000]. Considering only the eclogites with Ti/Sm > 3000 and Nb/Th > 24, and excluding all samples that lack data for all the elements of interest (Nb, Th, Ti, Sm, U, etc.), the average trace element composition of the TITAN-enriched eclogites of *Becker et al.* [2000] is Th = 0.159 ppm; U = 0.165 ppm; Nb = 10 ppm; Nd = 7.58 ppm; Sr = 88.7 ppm, Zr = 152 ppm, Sm = 2.16 ppm, Ti = 10,080 ppm.

3.4.2. The $^{187}Os/^{188}Os$ of Ancient, Lithospheric Peridotite and Refractory Eclogite

[19] The $^{187}Os/^{188}Os$ of DMM and Primitive Mantle are not very different (0.12–0.13 [*Standish et al.*, 2002; *Meisel et al.*, 2001]), and thus the isolated, ancient peridotite at the base of subducted plates are assumed to have an intermediate present-day composition (0.125). DMM and the subducted peridotites at the base of the oceanic lithosphere are also assumed to have had an Os concentration of 3000 ppt over geologic time. In contrast to the subducted lithospheric peridotite, the eclogitic portion of the subducted plate likely evolved extremely radiogenic $^{187}Os/^{188}Os$ over time (Figure 3). The $^{187}Os/^{188}Os$ evolution of the refractory eclogite is modeled using the median $^{187}Re/^{188}Os$ (325) and Os (6 ppt) values of eclogites that were metamorphosed in paleosubduction zones (see *Becker* [2000] for compositions). As shown in Figure 3, earlier subduction injection of eclogites with this present-day Re/Os ratio yield more radiogenic $^{187}Os/^{188}Os$ in the subducted eclogite reservoir. The high calculated present-day $^{187}Os/^{188}Os$ ratios in the recycled eclogites are similar to the most radiogenic eclogites presented by *Becker* [2000].

3.4.3. TITAN Anomalies of Ancient Lithospheric Peridotite and Refractory Eclogite

[20] The trace element content of the present-day peridotite from the base of the oceanic mantle lithosphere is assumed to be the same as the DMM compositions calculated by *Workman and Hart* [2005]. However, DMM has likely become increasingly depleted throughout geologic time. We assume that DMM began with a primitive mantle composition [*McDonough and Sun*, 1995] and evolved by continuous depletion until the present day. Using the continuous transport equations in Appendix A, the trace element budget of DMM is calculated at various times, and ''snapshots'' of DMM compositions through time are plotted as spidergrams in Figure 4 (see Table 3 for compositions). By contrast, the subducted eclogites are assumed to have the same present-day trace element composition as the hypothetical refractory eclogite from *McDonough* [1991], regardless of the isolation time (see Table 3). The composition of eclogite that has survived subduction zone processing is poorly constrained, and may exhibit significant compositional variability [e.g., *John et al.*, 2004; *Zack and John*, 2007]. However, the hypothetical eclogite from *McDonough* [1991] has a trace element composition similar to the eclogites with the largest positive TITAN anomalies presented by *Becker et al.* [2000], and is used for the modeling purposes here (see Table 3).

3.5. Model Results: Mixing Lithospheric Peridotite With Refractory Eclogite

[21] *Brandon et al.* [2007] showed that the moderately radiogenic $^{187}Os/^{188}Os$ observed in high $^{3}He/^{4}He$ Icelandic lavas can be explained by the presence of a recycled eclogite component in the dominantly peridotitic high $^{3}He/^{4}He$ mantle beneath Iceland. In addition to generating moderately radiogenic $^{187}Os/^{188}Os$ and high $^{3}He/^{4}He$ signatures, a mixture of ancient refractory eclogite and lithospheric peridotite can generate the positive TITAN anomalies seen in high $^{3}He/^{4}He$ OIB lavas. Given the parameters provided in Table 3, the model generates $^{3}He/^{4}He$, $^{187}Os/^{188}Os$ and positive TITAN anomalies that are most similar to the highest $^{3}He/^{4}He$ OIB lavas when the proportion of refractory eclogite in the mixture is between 20 and 25%, and the eclogite and peridotite have an age of 3 Ga (Figure 2). If the proportion of refractory eclogite is increased, the present-day $^{3}He/^{4}He$ in the resulting mixture is diminished and the positive TITAN anomalies and $^{187}Os/^{188}Os$ ratios are both increased to values above those observed in high $^{3}He/^{4}He$ OIB lavas. A smaller proportion of eclogite in the mixture will yield even higher $^{3}He/^{4}He$ ratios in the present day, but the TITAN anomalies and $^{187}Os/^{188}Os$ ratios will be lower than observed in high $^{3}He/^{4}He$ OIB lavas. On the other hand, if the eclogite and peridotite are younger than 3 Ga, the resulting mixture (20% eclogite and 80% peridotite) generates a $^{3}He/^{4}He$ ratio lower than observed in the highest $^{3}He/^{4}He$ OIB lavas (see the mixing curve for 1 Ga eclogite and peridotite in Figure 2). An eclogite-peridotite mixture of more ancient origin generates higher $^{3}He/^{4}He$ and $^{187}Os/^{188}Os$ ratios than identified in high $^{3}He/^{4}He$ OIB lavas. However, uncertainty in the composition of the hypothetic recycled eclogite makes it difficult to evaluate the precise proportion of eclogite in the high $^{3}He/^{4}He$ mantle. Thus, the result of 20–25% eclogite holds only for the refractory eclogite composition of *McDonough* [1991] and the assumed high $^{3}He/^{4}He$ peridotite composition given in Table 3.

[22] Figure 4 shows that the addition of 20% eclogite to a 3 Ga DMM composition generates a hybrid eclogite-peridotite spidergram that is similar

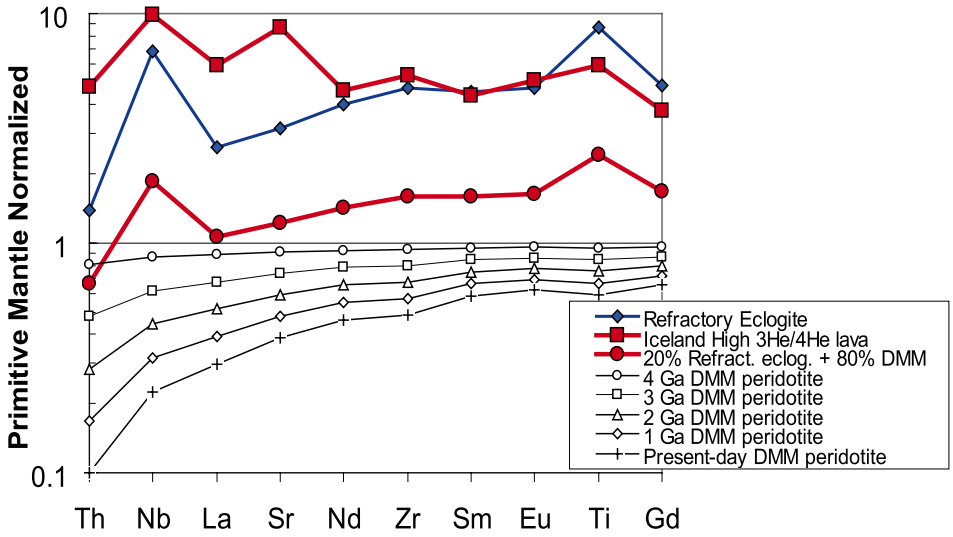

Figure 4. Spidergram of *McDonough's* [1991] refractory eclogite used in the modeling, including spidergrams demonstrating the time-dependent trace element composition of DMM. In the mixing models shown in Figure 2, the lithospheric peridotite and refractory eclogitic portions of a 3 Ga subducted plate are mixed together such that the final mixture has 20–25% eclogite. This mixing calculation is shown in the spidergram, where 20% ancient (3 Ga), refractory eclogite has been added to peridotite from the deepest portion of same age oceanic mantle lithosphere (with the same peridotite composition as DMM at 3 Ga). Refer to Table 3 for compositions of the 3 Ga refractory eclogite and the 3 Ga peridotite. Excluding Sr (see text for discussion of shallow lithospheric contamination and the resulting Sr-anomalies in some Icelandic lavas), the shape of the hybrid peridotite-eclogite spidergram, including the positive Nb and Ti anomalies, is very similar in shape to the spidergram of the high $^{3}He/^{4}He$ Icelandic lava. This similarity is consistent with the hybrid peridotite-eclogite being the source of the high $^{3}He/^{4}He$ mantle sample by OIBs.

in shape to the spidergram of the highest $^{3}He/^{4}He$ lava from Iceland. (Sr is a poor fit, however, due to the positive Sr anomalies in the Icelandic lava, a possible result of interaction with shallow lithospheric gabbros [*Gurenko and Sobolev*, 2006]). As long as the magnitude of TITAN anomalies is little affected by partial melting beneath a hot spot (i.e., the positive TITAN anomalies in the mantle source of high $^{3}He/^{4}He$ lavas are reflected in the erupted hot spot lavas), the hybrid eclogite-peridotite spidergram in Figure 4 may thus serve as a plausible melt source for the high $^{3}He/^{4}He$ lava. Clearly, this requires that the rutile present in the downgoing slab is no longer present in the high $^{3}He/^{4}He$ mantle that melts beneath hot spots. One way to destabilize rutile is to completely mix the (smaller proportion of) eclogite and the (larger proportion of) peridotite in the ancient recycled slab. Alternatively, if eclogite is still present in the source of the high $^{3}He/^{4}He$ OIB mantle source, it must be melted to a sufficiently high degree to eliminate rutile as a phase in the residue of melting (G. A. Gaetani et al., Titanium coordination and rutile saturation in eclogite partial melts at upper mantle conditions, submitted to *Earth and Planetary Science Letters*, 2007). Additionally, due to solid solution with other phases (e.g., garnet), the stability of rutile decreases with pressure, and may become exhausted during decompression melting [*Klemme et al.*, 2002].

[23] The model for the generation of high $^{3}He/^{4}He$, TITAN-enriched mantle can also generate a low $^{3}He/^{4}He$ mantle reservoir with positive TITAN anomalies. Subduction is a continuous process that has probably operated for much of geologic time, and the $^{3}He/^{4}He$ ratio of the upper mantle has likely decreased (Figure 3). Thus, the peridotite portion of more recently subducted oceanic plates will trap and preserve a lower $^{3}He/^{4}He$ upper mantle signature than ancient subducted plates. At the same time, the refractory eclogite portion of recently subducted plates will still host positive TITAN anomalies, such that low $^{3}He/^{4}He$ mantle reservoirs hosting TITAN anomalies can be generated by mixing more recently subducted (<2 Ga) peridotite and refractory eclogite components. For example, the lower $^{3}He/^{4}He$, TITAN-enriched mantle source sampled by Cape Verde lavas can be generated by mixing refractory eclogite (10–30% by mass) and lithospheric peridotite components of a plate subducted between 1 and 2 Ga (Figure 2).

[24] The "wedge-shaped" outline of the OIB data in Figure 2 highlights a striking absence of high $^3He/^4He$ lavas with negative (or even small positive) TITAN anomalies. Why do all high $^3He/^4He$ lavas exhibit TITAN-enrichment, or rather, why have high $^3He/^4He$-TITAN depleted (or only mildly TITAN enriched) lavas not been found? Continental crust and arc lavas (and associated sediments) compose the only known reservoir to exhibit TITAN depletion. Due to its extremely high U and Th contents, admixture of continental crust with high $^3He/^4He$ peridotite may not be conducive to the preservation of high $^3He/^4He$ [*Jackson et al.*, 2007a], and could explain why TITAN-depleted lavas always exhibit low $^3He/^4He$ (Figure 2). OIB lavas lacking TITAN anomalies may host an eclogite component that was not U and Th-depleted (and thus did not acquire positive TITAN anomalies) in a subduction zone, and may also produce significant ^4He.

[25] The observation that all high $^3He/^4He$ lavas exhibit TITAN anomalies may be explained by the intimate spatial and temporal association between the TITAN-enriched eclogites and high $^3He/^4He$ peridotites suggested by this model: The peridotite and refractory eclogite components (the raw materials for the formation of the high $^3He/^4He$, TITAN-enriched mantle) are always joined together in subducting plates, and it may not be possible to melt pure high $^3He/^4He$ peridotite without also melting some eclogite. This will be true particularly if subducted slabs are stretched, thinned and folded in the dynamic mantle [*Allègre and Turcotte*, 1986], such that the diminished thickness of the (eclogite and peridotite) slab is less than the width and depth of melting zones beneath hot spots. Such a process might explain why an eclogite signature (positive TITAN anomalies and radiogenic $^{187}Os/^{188}Os$) is invariably present in high $^3He/^4He$ lavas.

3.6. Two Alternative Models for a Hybrid High $^3He/^4He$ Mantle: "Eclogite Injection" and Diffusion of "Ghost" Primordial Helium

[26] An alternative process for generating the hybrid eclogite-peridotite high $^3He/^4He$ mantle assumes that subducted slab peridotite contributes little to the helium budget of the high $^3He/^4He$ mantle sampled by OIBs. Instead, the refractory slab eclogite penetrates into the lower mantle and mixes with a hypothetical lower mantle high $^3He/^4He$ (primitive and undegassed?) peridotite reservoir (i.e., not associated with the peridotite portion of slabs). The hybrid mixture then rises in a plume where it is melted beneath a hot spot. By comparison to the slab peridotite-eclogite "package" model describe in section 3.4 and 3.5 above, this alternative "eclogite injection" model does not guarantee an intimate spatial and temporal association of the high $^3He/^4He$ peridotite and TITAN-enriched eclogite components. For example, deep (primitive) mantle high $^3He/^4He$ peridotites could upwell in a plume without first mixing with refractory eclogite, in which case the erupted high $^3He/^4He$ lavas would lack positive TITAN anomalies. Such lavas have not been observed.

[27] Instead of mechanically mixing the high $^3He/^4He$ peridotite and TITAN-enriched eclogite, as suggested in the "slab package" and "eclogite injection" models above, it may be possible to diffusively mix helium from a high $^3He/^4He$ peridotite into a degassed, U and Th-poor pyroxenite (i.e., refractory eclogite) [*Albarede and Kaneoka*, 2007]. Due to the higher diffusivity of helium compared to nonvolatile major and trace elements [*Hart*, 1984; *Trull and Kurz*, 1993], helium isotopes may become decoupled from other lithophile isotope tracers [*Hart et al.*, 2007, 2008], and primordial helium may become associated with recycled materials like refractory eclogites [*Albarede and Kaneoka*, 2007]. *Albarede and Kaneoka* [2007] propose that helium from deep (high $^3He/^4He$) mantle peridotites can diffuse into embedded, tightly folded layers of stretched and thinned refractory eclogite. They suggest that changing the duration of the diffusion process, as well as the U and Th contents of the refractory eclogite layers, can generate mantle sources for both high and low $^3He/^4He$ hot spots. U and Th-poor refractory eclogite that was processed in subduction zones will have positive TITAN anomalies [*McDonough*, 1991], and because such eclogites will produce little ^4He over time, they are perfect "containers" for preserving diffusively acquired high $^3He/^4He$ signatures. If these eclogites become sufficiently thinned (to <1–2 km thickness) by mantle mixing, they could acquire high $^3He/^4He$ signatures by diffusion from the ambient deep mantle peridotite [*Hart et al.*, 2007, 2008]. Thus, the "ghost" helium model of *Albarede and Kaneoka* [2007] may offer a resolution to the paradoxical association of high $^3He/^4He$ signatures in lavas with strong eclogite signatures. However, the "ghost helium" model suffers from the same spatial and temporal issues as the "eclogite injection" model: There is no obvious mechanism

preventing ambient lower mantle (eclogite-free) peridotite with high $^3He/^4He$ from upwelling and melting beneath a hot spot, thus generating high $^3He/^4He$ lavas that lack positive TITAN anomalies.

3.7. High $^3He/^4He$ Lavas Without Positive TITAN Anomalies?

[28] If a high $^3He/^4He$ peridotite could be melted in pure (no eclogite) form, available partitioning data suggest that there would be no positive TITAN-anomalies in the erupted lavas. There would also be no contribution of ^4He ingrowth from the eclogite, and $^3He/^4He$ ratios higher than that observed in OIBs might be expected in the melts of such a mantle source. Such lavas have not been identified. However, with the highest magmatic $^3He/^4He$ values on record (up to ~50 Ra), Baffin Island lavas [*Stuart et al.*, 2003] may provide an important test case for this hypothesis, but trace element data on these lavas are not yet available.

4. TITAN Anomalies Due to Partitioning Between Lower Mantle Phases?

[29] It is difficult to rule out the possibility of TITAN fractionation in lower mantle materials, a mechanism that could produce the positive TITAN anomalies in the mantle sampled by high $^3He/^4He$ OIBs. Experimental studies of high pressure partitioning and mineralogy are in the early phases. However, Ca-perovskite in peridotitic and basaltic systems shows negative Ti and Nb partitioning patterns compared to Th, U, and the rare earth elements (REEs) [*Hirose et al.*, 2004]. This means that a Ca-perovskite bearing solid assemblage would have negative anomalies, but melt equilibrated with Ca-perovskite could have positive anomalies. If it is possible to generate Ca-perovskite melts at the appropriate pressures and temperatures (for example, D″), and extract them from the lower mantle (the inferred home of the high $^3He/^4He$ domain) in plumes, then Ca-perovskite melting in the lower mantle may offer a potential explanation for the origin of TITAN-enriched, high $^3He/^4He$ lavas.

5. High $^3He/^4He$, TITAN-Enriched Mantle: A Reservoir for the "Missing" TITAN Elements in the Earth?

[30] A shortage of the TITAN elements exists in the Earth's shallow geochemical reservoirs (the depleted MORB mantle (DMM) and continental crust), and the location of these missing elements is unknown. The standard model for the evolution of the silicate earth maintains that DMM is the residue of continental crust extraction from an early primitive mantle [*Jacobsen and Wasserburg*, 1979; *O'Nions et al.*, 1979; *Allègre et al.*, 1980; *Hofmann*, 1988, 1997]. If the bulk silicate earth has chondritic abundances of the refractory elements, DMM and continental crust must be geochemically complementary reservoirs within the Earth. However, the TITAN trio of elements are prominently depleted in the continents [*Rudnick and Gao*, 2003], and their absence is not balanced by a corresponding enrichment in DMM [*Workman and Hart*, 2005] (Figure 1). Thus, another deeper reservoir hosting the missing TITAN elements has been proposed to exist in the Earth [*McDonough*, 1991; *Rudnick et al.*, 2000; *Kamber and Collerson*, 2000].

[31] While incompatible elements are largely lost to the overlying mantle during dehydration and melting of the eclogite portion of downgoing slabs, titanium-rich phases, such as rutile, may preferentially sequester the TITAN elements in the mafic portion of downgoing slabs [*Green and Pearson*, 1986; *Ryerson and Watson*, 1987; *Brenan et al.*, 1994; *Foley et al.*, 2000; *Schmidt et al.*, 2004; *Kessel et al.*, 2005]. Refractory, rutile-bearing eclogites have been subducted in large quantities over geologic time, and may form a reservoir in the mantle that hosts part of the Earth's missing TITAN [*McDonough*, 1991; *Rudnick et al.*, 2000]. Upwelling regions of the mantle are thought to sample subducted eclogites [*Hofmann and White*, 1980, 1982; *Chase*, 1981]. If the high $^3He/^4He$ reservoir hosts a component of TITAN-enriched, refractory eclogite, then high $^3He/^4He$ OIBs may provide information about the location and composition of the reservoir hosting part of the Earth's missing TITAN elements.

[32] However, the high $^3He/^4He$ mantle alone may not entirely satisfy the requirements for the reservoir hosting the Earth's missing TITAN. Shallow geochemical reservoirs in the Earth, continental crust and DMM, exhibit subchondritic Nb/Ta ratios, and another terrestrial reservoir with superchondritic Nb/Ta is required if the Earth has chondritic abundances of the refractory elements. Recycled, refractory eclogites may have superchondritic Nb/Ta ratios, and have been suggested to host the Earth's missing superchondritic Nb/Ta [*McDonough*, 1991; *Rudnick et al.*, 2000; *Kamber*

and Collerson, 2000]. If high $^{3}He/^{4}He$ lavas sample such a reservoir, they should exhibit high Nb/Ta ratios, but all such lavas exhibit subchondritic Nb/Ta (see Table 1). One resolution to this issue may be that bulk silicate earth is not chondritic. It has been proposed that an initially chondritic silicate earth may have lost Nb to the core, and that the core is the reservoir hosting the "missing" superchondritic Nb/Ta [*Wade and Wood*, 2001; *Münker et al.*, 2003]. If this is the case, then the combined budgets of the TITAN elements in the core and the high $^{3}He/^{4}He$ mantle reservoir may balance the Earth's budget for the TITAN elements, a hypothesis that may help resolve the lack of geochemical complementarity between DMM and continental crust.

6. Conclusions

[33] From this study, we draw the following conclusions:

[34] 1. High $^{3}He/^{4}He$ OIB lavas exhibit enrichment (or positive anomalies) in Ti, Ta and Nb (TITAN) relative to elements of similar compatibility.

[35] 2. High $^{3}He/^{4}He$ OIBs exhibit moderately radiogenic $^{187}Os/^{188}Os$ (>0.135). The $^{187}Os/^{188}Os$ ratios found in high $^{3}He/^{4}He$ lavas greatly exceeds that found in DMM (0.120–0.125) or primitive mantle (0.129).

[36] 3. One feasible explanation for the high $^{3}He/^{4}He$, TITAN enrichment and moderately radiogenic $^{187}Os/^{188}Os$ is the addition of 20–25% refractory, ancient (3 Ga) eclogite to a high $^{3}He/^{4}He$ peridotite of the same age. The association of the refractory eclogite signature with high $^{3}He/^{4}He$ (>30 Ra) lavas suggests an intimate spatial and temporal association of the eclogite and peridotite portions of the high $^{3}He/^{4}He$ reservoir. The eclogite and peridotite portions of the high $^{3}He/^{4}He$ domain are modeled as being part of the same, ancient subducted slab that remained together as a package in space and time. This intimate association of the eclogite and peridotite components is required. Otherwise, high $^{3}He/^{4}He$ lower mantle peridotites could upwell without first being inoculated with TITAN-enriched eclogite, and the resulting high $^{3}He/^{4}He$ melts of such an eclogite-free source would not exhibit positive TITAN anomalies. Such lavas have not been observed.

[37] 4. Due to the paucity of high pressure experimental trace element partitioning data, the generation of TITAN anomalies by partitioning between lower mantle phases cannot be ruled out. For example, extant experimental data suggest that melts of Ca-perovskite are TITAN enriched. Thus, we cannot exclude the possibility that the high $^{3}He/^{4}He$ mantle sampled by OIBs hosts a component of melt derived from melting Ca-perovskite.

[38] 5. Together with the core, the high $^{3}He/^{4}He$, TITAN-enriched mantle domain may host the missing TITAN elements in the Earth, and may help explain the lack of geochemical complementarity between DMM and continental crust.

Appendix A: Helium Isotope Model

[39] The precise timing of the genesis of the high $^{3}He/^{4}He$ reservoirs cannot be calculated using helium isotopes because the degassing history and present-day ^{3}He content of the DMM reservoir, as well as the initial $^{4}He/^{3}He$ and ^{3}He budgets of the undegassed mantle, are not well known. Thus, the age of the high $^{3}He/^{4}He$ reservoir sampled by OIB lavas is poorly constrained.

[40] One possible model for the time evolution of $^{3}He/^{4}He$ in DMM and primitive mantle is as follows. Assuming $^{238}U/^{3}He$ and $^{3}He/^{4}He$ ratios for the undegassed mantle as given in Table 3, and assuming that DMM was formed by continuous depletion by extraction of oceanic and continental crust from a chondritic primitive mantle over Earth's history, the known $^{3}He/^{4}He$ of present-day DMM (8 Ra) can be used to calculate the present-day $^{238}U/^{3}He$ of DMM. Employing the continuous transport equations [*Allègre*, 1968; *Hart and Brooks*, 1970; *Workman and Hart*, 2005] to describe the continuously depleting upper mantle (DMM), the $^{238}U/^{3}He$ and $^{3}He/^{4}He$ of DMM can be calculated at any time from 4.4 Ga to the present day (see Table 3 for a list of these values for DMM at different times in Earth's history). The helium isotope evolution of the continuously depleting DMM reservoir is modeled using the following continuous transport equations (see Figure 3):

$$\begin{aligned}{}^{4}He/^{3}He_{t} = {}& {}^{4}He/^{3}He_{T} + 8\lambda_{238}/(\lambda_{238}+k_{238})\left({}^{238}U/^{3}He\right)_{T} \\ & \cdot (1-\exp(-1(T-t)(\lambda_{238}+k_{238}))) \\ & + 7\lambda_{235}/(\lambda_{235}+k_{235})\left({}^{235}U/^{3}He\right)_{T} \\ & \cdot (1-\exp(-1(T-t)(\lambda_{235}+k_{235}))) \\ & + 6\lambda_{232}/(\lambda_{232}+k_{232})\left({}^{232}Th/^{3}He\right)_{T} \\ & \cdot (1-\exp(-1(T-t)(\lambda_{232}+k_{232}))) \end{aligned} \quad \text{(A1)}$$

where

$$k_{238} = -1 \ln\left(\left(^{238}U/^{3}He\right)_0/\left(^{238}U/^{3}He\right)_T\right)/(T-t) - \lambda_{238}; \quad (A2)$$

$$k_{235} = -1 \ln\left(\left(^{235}U/^{3}He\right)_0/\left(^{235}U/^{3}He\right)_T\right)/(T-t) - \lambda_{235}; \quad (A3)$$

$$k_{232} = -1 \ln\left(\left(^{232}Th/^{3}He\right)_0/\left(^{232}Th/^{3}He\right)_T\right)/(T-t) - \lambda_{232} \quad (A4)$$

where λ_{238} (1.55×10^{-10} a^{-1}), λ_{235} (9.85×10^{-10} a^{-1}) and λ_{232} (4.95×10^{-11} a^{-1}) are the decay constants for ^{238}U, ^{235}U, and ^{232}Th, respectively, and k_{238}, k_{235} and k_{232} are the continuous transport coefficients for the U-Th-He system in DMM. T is the starting time of the model (4.4 Ga), and "t" is the time before the present day (and T-t equals elapsed time). The k-value is the difference in transport coefficients for U (or Th) and He, and is related to the difference in bulk partition coefficients between U (or Th) and He; negative k-values in the model indicate that He is transported from the mantle more efficiently than U and Th.

[41] When $k_{238,235,232}$ equals zero, equations (A1)–(A4) describe closed-system $^{3}He/^{4}He$ evolution. It is assumed that the undegassed mantle has been closed to degassing since 4.4 Ga. Thus, the closed-system model starts at time t = 4.4 Ga. The $^{4}He/^{3}He_T$ (initial ratio) of primitive mantle is unconstrained, but is assumed to be 5,995 (or 120 Ra) and is assumed to increase to 7,224 (or ~100 Ra) today. The $^{232}Th/^{238}U_0$ (present-day) ratio of primitive mantle is assumed to be 4.05 [*McDonough and Sun*, 1995]. Using U concentrations for primitive mantle from *McDonough and Sun* [1995], the primitive mantle $^{238}U/^{3}He_0$ (present-day) ratio is then 70. A higher $^{238}U/^{3}He$ value for primitive mantle would require a lower primitive mantle $^{3}He/^{4}He$ ratio and ^{3}He abundance. The DMM reservoir derived from such a ^{3}He-poor primitive mantle would in turn have a lower ^{3}He abundance and generate lithospheric peridotites with lower ^{3}He abundances. The lower ^{3}He abundances of such lithospheric peridotites would be less able to preserve high $^{3}He/^{4}He$ in the presence of ^{4}He-producing, refractory eclogites. Thus, in order to generate the present-day $^{3}He/^{4}He$ observed in the high $^{3}He/^{4}He$ OIB reservoir, either smaller amounts of eclogite could be tolerated (<20%, which would result in insufficiently large TITAN anomalies and radiogenic $^{187}Os/^{188}Os$), or the lithospheric peridotite-eclogite package would have to be formed earlier (i.e., before 3 Ga, when DMM had suffered less degassing and had higher ^{3}He abundances).

[42] From the $^{238}U/^{3}He_0$ ratio, the ^{3}He can be calculated by employing a present-day primitive mantle U concentration of 0.0203 ppm [*McDonough and Sun*, 1995], and is 7.3×10^{11} atoms/g. This ^{3}He value is somewhat higher than the planetary component found in meteorites (<1×10^{11} atoms/g), but lower than the ^{3}He abundance (~1×10^{12} atoms/g) suggested for an early isolated, rare-gas-bearing reservoir above the core mantle boundary (or D″) [*Tolstikhin and Hofmann*, 2005]. Our preferred primitive mantle ^{3}He concentration is higher than the minimum ^{3}He concentration (~1×10^{11} atoms/g), a value that is obtained by assuming that primitive mantle has a minimum $^{3}He/^{4}He$ of 50 Ra (the highest magmatic $^{3}He/^{4}He$ on record [*Stuart et al.*, 2003]) and a U concentration similar to that provided by *McDonough and Sun* [1995]. Note that noble gas concentrations in the deep Earth, and in the early Earth, are poorly constrained, so this is an important uncertainty in the model calculations.

[43] The model for the $^{3}He/^{4}He$ and $^{238}U/^{3}He$ of DMM starts at time t = 4.4 Ga. It is assumed that DMM and primitive mantle had the same composition ($^{4}He/^{3}He_T$, $^{238}U/^{3}He_T$ and $^{232}Th/^{238}U_T$) at 4.4 Ga, and that DMM began forming immediately by melt extraction from primitive mantle starting at 4.4 Ga. It is further assumed that DMM has evolved to exhibit present-day $^{232}Th/^{238}U_0$ and $^{4}He/^{3}He_0$ values of 2.55 (similar to the value for average DMM of *Workman and Hart* [2005]) and ~89,900 (8 Ra), respectively. Equations (A1) through (A4) are then solved for $^{238}U/^{3}He_0$, which is calculated to be ~54,000. For this solution, k_{238} and k_{235} are both -1.51×10^{-9} a^{-1} and k_{232} is -1.41×10^{-9} a^{-1}. If a DMM U concentration of 0.0032 ppm is assumed [*Workman and Hart*, 2005], the ^{3}He of present-day DMM is calculated to be 1.5×10^{8} atoms/g.

[44] The ^{3}He abundance in DMM calculated with the continuous depletion model is within a factor of 3 to 20 of the ^{3}He abundances inferred from MORB samples and ^{3}He flux from ridges (see *Ballentine et al.* [2002] for summary). Assuming 10% melting of the mantle source, ^{3}He concentrations for DMM were derived from CO_2 concentrations and canonical mantle $CO_2/^{3}He$ ratios in MORB melt inclusions ($4.52 \times 10^{8} \pm 1.93$ atoms

^{3}He/g [*Saal et al.*, 2002], "popping" rock (>2.69 × 10^9 atoms ^{3}He/g [*Moreira et al.*, 1998]), and flux of ^{3}He out of mid-ocean ridges (1.18 × 10^9 atoms ^{3}He/g [*Farley et al.*, 1995; *Ballentine et al.*, 2002]). The estimates for DMM ^{3}He derived from popping rock and ^{3}He flux from ridges come to closer agreement with our ^{3}He model results if vast regions of DMM (down to ~330 km depth) suffer from the low degree carbonatite melting, as suggested by the experiments of *Dasgupta and Hirschmann* [2006].

[45] The increase in ^{238}U/^{3}He in DMM over the age of the Earth (Table 3) requires that He is less compatible than U and Th during melting of this mantle reservoir. The assumption of increased ^{238}U/^{3}He in DMM over time is realistic given the lherzolitic lithology of DMM, a mantle reservoir that hosts an estimated cpx modal abundance of ~13% [*Workman and Hart*, 2005]. Results from a recent helium partitioning study [*Heber et al.*, 2007] are consistent with helium being less compatible than U and Th (assuming U and Th partition coefficients from a recent compilation [*Kelemen et al.*, 2003]) during mantle melting of a lherzolite lithology. However, helium partitioning during mantle melting is a controversial subject. *Parman et al.* [2005] reported olivine-melt partition coefficients for helium suggesting that helium may be more compatible than U and Th during melting of a cpx-poor lherzolite or harzburgite. By contrast, *Heber et al.* [2007] report values that are over an order of magnitude smaller (less compatible), suggesting the helium may be more compatible than U and Th only when melting cpx-poor harzburgites or dunites. The discrepancy in olivine-melt helium partition coefficients between these two studies is not yet resolved.

[46] The continuous transport equations can be written to calculate the concentrations of any element in DMM at any time in Earth's history, assuming that DMM formed by continuous depletion of BSE starting at 4.4 Ga:

$$X_{DMM,t} = X_{BSE,0}(\exp(-1(\alpha_X)[T - t])) \quad (A5)$$

where

$$\alpha_X = -1 \ln(X_{DMM,0}/X_{BSE,0})/(T) \quad (A6)$$

where α_X is proportional to the transport of element X out of DMM over time; $X_{BSE,0}$ and $X_{DMM,0}$ are the present-day concentrations of element X in BSE and DMM, respectively; "t" is time before the present day and t = 4.4 Ga, and $X_{DMM,t}$ is the concentration of element X in DMM at any time "t" before the present day. Using equations (A5) and (A6), concentrations of trace elements that are known in BSE and present-day DMM can be used to calculate their time-dependent concentrations in DMM. For example, the present-day Ti concentrations in DMM (716 ppm) and BSE (1205 ppm) yield an α_{Ti} value of 1.18 × 10^{-10} a^{-1} in equation (A6). Thus, using this α_{Ti} value and solving for $Ti_{DMM,t}$ in equation (A6), the concentration of Ti in DMM can be calculated at any time in Earth's history. More incompatible elements have larger values for α. For example, α_{Th} = 5.25 × 10^{-10} a^{-1} and α_U = 4.20 × 10^{-10} a^{-1}, where Th is more incompatible than U. In Table 3, the abundances of several trace elements in DMM are provided at various times in Earth's history.

Acknowledgments

[47] L. Ball's assistance with our resident titan, WHOI's ThermoFinnigan Neptune, was invaluable for the success of this work. We would like to thank D. Hilton and P. Castillo for generously providing their Iceland sample for trace element analysis. We thank S. Mukhopadhyay, R. Rudnick, and C. Münker for helpful reviews and V. Salters for editorial handling. Discussion with Z. Wang, E. Hauri, A. Shaw, P. Kelemen, K. Sims, and F. Frey is gratefully acknowledged. Funds for helium measurements were provided by NSF-OCE to M.D.K. Funds for major and trace element analyses were provided by NSF-EAR 0509891 to S.R.H.

References

Abedini, A. A., S. Hurwitz, and W. C. Evans (2006), USGS-NoGaDat — A global dataset of noble gas concentrations and their isotopic ratios in volcanic systems*U.S. Geol. Surv. Digital Data Ser.*, *202*. (Available at http://pubs.usgs.gov/ds/2006/202).

Albarede, F., and I. Kaneoka (2007), Ghost primordial He and Ne, paper presented at 17th Annual Goldschmidt Conference, Eur. Assoc. for Geochem., Cologne, Germany.

Allègre, C. J. (1968), Comportement des systemes U-Th-Pb dans le manteau superieur et modele d'evolution de ce dernier au cours des temps geologiques, *Earth Planet. Sci. Lett.*, *5*, 261–269, doi:10.1016/S0012-821X(68)80050-0.

Allègre, C. J., and D. L. Turcotte (1986), Implications of a two-component marble-cake mantle, *Nature*, *323*, 123–127, doi:10.1038/323123a0.

Allègre, C. J., O. Brévart, B. Dupré, and J. F. Minster (1980), Isotopic and chemical effects produced in a continuously differentiating convecting earth mantle, *Philos. Trans. R. Soc. London, Ser. A*, *297*, 447–477, doi:10.1098/rsta.1980.0225.

Allègre, C. J., T. Staudacher, P. Sarda, and M. Kurz (1983), Constraints on evolution of Earth's mantle from rare gas systematics, *Nature*, *303*, 762–766, doi:10.1038/303762a0.

Anderson, D. L. (1998), A model to explain the various paradoxes associated with mantle noble gas geochemistry, *Proc.*

Natl. Acad. Sci. U. S. A., *95*, 9087–9092, doi:10.1073/pnas.95.16.9087.

Ayers, J. (1998), Trace element modeling of aqueous fluid–peridotite interaction in the mantle wedge of subduction zones, *Contrib. Mineral. Petrol.*, *132*, 390–404, doi:10.1007/s004100050431.

Ballentine, C. J., P. E. van Keken, D. Porcelli, and E. H. Hauri (2002), Numerical models, geochemistry and the zero-paradox noble-gas mantle, *Philos. Trans. R. Soc. London, Ser. A*, *360*, 2611–2631, doi:10.1098/rsta.2002.1083.

Becker, H. (2000), Re-Os fractionation in eclogites and blueschists and the implications for recycling of oceanic crust into the mantle, *Earth Planet. Sci. Lett.*, *177*, 287–300, doi:10.1016/S0012-821X(00)00052-2.

Becker, H., K. P. Jochum, and R. W. Carlson (2000), Trace element fractionation during dehydration of eclogites from high-pressure terranes and the implications for element fluxes in subduction zones, *Earth Planet. Sci. Lett.*, *163*, 65–99.

Brandon, A. D., R. A. Creaser, S. B. Shirey, and R. W. Carlson (1996), Osmium recycling in subduction zones, *Science*, *272*, 861–864, doi:10.1126/science.272.5263.861.

Brandon, A. D., D. W. Graham, T. Waight, and B. Gautason (2007), ^{186}Os and ^{187}Os enrichments and high $^{3}He/^{4}He$ sources in the Earth's mantle: Evidence from Icelandic picrites, *Geochim. Cosmochim. Acta*, *71*, 4570–4591, doi:10.1016/j.gca.2007.07.015.

Breddam, K. (2002), Kistufell: Primitive melt from the Icelandic mantle plume, *J. Petrol.*, *43*, 345–373, doi:10.1093/petrology/43.2.345.

Breddam, K., M. D. Kurz, and M. Storey (2000), Mapping out the conduit of the Icelandic mantle plume with helium isotopes, *Earth Planet. Sci. Lett.*, *176*, 45–55, doi:10.1016/S0012-821X(99)00313-1.

Brenan, J. M., H. F. Shaw, D. L. Phinney, and F. J. Ryerson (1994), Rutile-aqueous fluid partitioning of Nb, Ta, Hf, Zr, U and Th: Implications for high field strength element depletions in island-arc basalts, *Earth Planet. Sci. Lett.*, *128*, 327–339, doi:10.1016/0012-821X(94)90154-6.

Chase, C. G. (1981), Oceanic island Pb: Two-stage histories and mantle evolution, *Earth Planet. Sci. Lett.*, *52*, 277–284, doi:10.1016/0012-821X(81)90182-5.

Chauvel, C., A. W. Hofmann, and P. Vidal (1992), HIMU-EM: The French-Polynesian connection, *Earth Planet. Sci. Lett.*, *110*, 99–119, doi:10.1016/0012-821X(92)90042-T.

Class, C., and S. L. Goldstein (2005), Evolution of helium isotopes in the Earth's mantle, *Nature*, *436*, 1107–1112, doi:10.1038/nature03930.

Dasgupta, R., and M. M. Hirschmann (2006), Melting of the Earth's deep upper mantle caused by carbon dioxide, *Nature*, *440*, 659–662, doi:10.1038/nature04612.

Dixon, J. E., L. Leist, C. Langmuir, and J. G. Schilling (2002), Recycled dehydrated lithosphere observed in plume-influenced mid-ocean-ridge basalt, *Nature*, *420*, 385–389, doi:10.1038/nature01215.

Farley, K. A., J. H. Natland, and H. Craig (1992), Binary mixing of enriched and undegassed (primitive?) mantle components (He, Sr, Nd, Pb) in Samoan lavas, *Earth Planet. Sci. Lett.*, *111*, 183–199, doi:10.1016/0012-821X(92)90178-X.

Farley, K. A., E. Maierreimer, P. Schlosser, and W. S. Broecker (1995), Constraints on mantle He-3 fluxes and deep-sea circulation from an oceanic general circulation model, *J. Geophys. Res.*, *100*, 3829–3839, doi:10.1029/94JB02913.

Fitton, J. G., A. D. Saunders, M. J. Norry, B. S. Hardarson, and R. N. Taylor (1997), Thermal and chemical structure of the Iceland plume, *Earth Planet. Sci. Lett.*, *153*, 197–208, doi:10.1016/S0012-821X(97)00170-2.

Foley, S. F., M. G. Barth, and G. A. Jenner (2000), Rutile/melt partition coefficients for trace elements and an assessment of the influence of rutile on the trace element characteristics of subduction zone magmas, *Geochim. Cosmochim. Acta*, *64*, 933–938, doi:10.1016/S0016-7037(99)00355-5.

Frey, F. A., and D. A. Clague (1983), Geochemistry of diverse basalt types from Loihi Seamount, Hawaii: Petrogenetic implications, *Earth Planet. Sci. Lett.*, *66*, 337–355, doi:10.1016/0012-821X(83)90150-4.

Graham, D. W., S. E. Humphris, W. J. Jenkins, and M. D. Kurz (1992), Helium isotope geochemistry of some volcanic rocks from Saint Helena, *Earth Planet. Sci. Lett.*, *110*, 121–131, doi:10.1016/0012-821X(92)90043-U.

Green, T. H., and N. J. Pearson (1986), Ti-rich accessory phase saturation in hydrous mafic-felsic compositions at high P,T, *Chem. Geol.*, *54*, 185–201, doi:10.1016/0009-2541(86)90136-1.

Gurenko, A. A., and A. V. Sobolev (2006), Crust–primitive magma interaction beneath neovolcanic rift zone of Iceland recorded in gabbro xenoliths from Midfell, SW Iceland, *Contrib. Mineral. Petrol.*, *151*, 495–520, doi:10.1007/s00410-006-0079-2.

Hanan, B. B., and D. W. Graham (1996), Lead and helium isotope evidence from oceanic basalts for a common deep source of mantle plumes, *Science*, *272*, 991–995, doi:10.1126/science.272.5264.991.

Hanyu, T., and I. Kaneoka (1997), The uniform and low $^{3}He/^{4}He$ ratios of HIMU basalts as evidence for their origin as recycled materials, *Nature*, *390*, 273–276, doi:10.1038/36835.

Hart, S. R. (1984), He diffusion in olivine, *Earth Planet. Sci. Lett.*, *70*, 297–302, doi:10.1016/0012-821X(84)90014-1.

Hart, S. R., and C. Brooks (1970), Rb-Sr mantle evolution models, *Year Book Carnegie Inst. Washington*, *68*, 426–429.

Hart, S. R., and G. A. Gaetani (2006), Mantle Pb paradoxes: the sulfide solution, *Contrib. Mineral. Petrol.*, *152*, 295–308, doi:10.1007/s00410-006-0108-1.

Hart, S. R., E. H. Hauri, L. A. Oschmann, and J. A. Whitehead (1992), Mantle plumes and entrainment: Isotopic evidence, *Science*, *256*, 517–520, doi:10.1126/science.256.5056.517.

Hart, S. R., J. Blusztajn, H. J. B. Dick, P. S. Meyer, and K. Muehlenbachs (1999), The fingerprint of seawater circulation in a 500-meter section of oceanic crust gabbros, *Geochim. Cosmochim. Acta*, *63*, 4059–4080, doi:10.1016/S0016-7037(99)00309-9.

Hart, S. R., M. D. Kurz, and Z. Wang (2007), Scale length of mantle heterogeneities: Helium diffusion constraints, *Eos Trans. AGU*, *88*(52), Fall Meet. Suppl., Abstract U21B-0407.

Hart, S. R., M. D. Kurz, and Z. Wang (2008), Scale length of mantle heterogeneities: Constraints from He diffusion, *Earth Planet. Sci. Lett.*, doi:10.1016/j.epsl.2008.03.010, in press.

Hauri, E. H. (1996), Major element variability in the Hawaiian plume, *Nature*, *382*, 415–419.

Hauri, E. H., and S. R. Hart (1993), Re-Os isotope systematics of HIMU and EMII oceanic island basalts from the south Pacific Ocean, *Earth Planet. Sci. Lett.*, *114*, 353–371, doi:10.1016/0012-821X(93)90036-9.

Heber, V. S., R. A. Brooker, S. P. Kelley, and B. J. Wood (2007), Crystal-melt partitioning of noble gases (helium, neon, argon, krypton, and xenon) for olivine and clinopyroxene, *Geochim. Cosmochim. Acta*, *71*, 1041–1061, doi:10.1016/j.gca.2006.11.010.

Hilton, D. R., K. Grönvold, C. G. Macpherson, and P. R. Castillo (1999), Extreme $^3He/^4He$ ratios in northwest Iceland: Constraining the common component in mantle plumes, *Earth Planet. Sci. Lett.*, *173*, 53–60, doi:10.1016/S0012-821X(99)00215-0.

Hirose, K., N. Shimizu, W. van Westrenen, and Y. Fei (2004), Trace element partitioning in Earth's lower mantle and implications for geochemical consequences of partial melting at the core-mantle boundary, *Phys. Earth Planet. Inter.*, *146*, 249–260, doi:10.1016/j.pepi.2002.11.001.

Hofmann, A. W. (1988), Chemical differentiation of the Earth: The relationship between mantle, continental crust, and oceanic crust, *Earth Planet. Sci. Lett.*, *90*, 297–314, doi:10.1016/0012-821X(88)90132-X.

Hofmann, A. W. (1997), Mantle geochemistry: The message from oceanic volcanism, *Nature*, *385*, 219–229, doi:10.1038/385219a0.

Hofmann, A. W., and W. M. White (1980), The role of subducted oceanic crust in mantle evolution, *Year Book Carnegie Inst. Washington*, *79*, 477–483.

Hofmann, A. W., and W. M. White (1982), Mantle plumes from ancient oceanic crust, *Earth Planet. Sci. Lett.*, *57*, 421–436, doi:10.1016/0012-821X(82)90161-3.

Hofmann, A. W., K. P. Jochum, M. Seufert, and W. M. White (1986), Nb and Pb in oceanic basalts: New constraints on mantle evolution, *Earth Planet. Sci. Lett.*, *79*, 33–45, doi:10.1016/0012-821X(86)90038-5.

Honda, M., and J. D. Woodhead (2005), A primordial solar-neon enriched component in the source of EM-I-type ocean island basalts from the Pitcairn Seamounts, Polynesia, *Earth Planet. Sci. Lett.*, *236*, 597–612, doi:10.1016/j.epsl.2005.05.038.

Jackson, M. G., S. R. Hart, A. A. P. Koppers, H. Staudigel, J. Konter, J. Blusztajn, M. D. Kurz, and J. A. Russell (2007a), The return of subducted continental crust in Samoan lavas, *Nature*, *448*, 684–697, doi:10.1038/nature06048.

Jackson, M. G., M. D. Kurz, S. R. Hart, and R. K. Workman (2007b), New Samoan lavas from Ofu Island reveal a hemispherically heterogeneous high $^3He/^4He$ mantle, *Earth Planet. Sci. Lett.*, *264*, 360–374, doi:10.1016/j.epsl.2007.09.023.

Jacobsen, S. B., and G. J. Wasserburg (1979), The mean age of mantle and crustal reservoirs, *J. Geophys. Res.*, *84*, 7411–7427.

John, T., E. E. Scherer, K. Haase, and V. Schenk (2004), Trace element fractionation during fluid-induced eclogitization in a subducting slab: Trace element and Lu-Hf-Sm-Nd isotope systematics, *Earth Planet. Sci. Lett.*, *227*, 441–456, doi:10.1016/j.epsl.2004.09.009.

Kamber, B. S., and K. D. Collerson (2000), Role of "hidden" deeply subducted slabs in mantle depletion, *Chem. Geol.*, *166*, 241–254, doi:10.1016/S0009-2541(99)00218-1.

Kelemen, P. B., N. Shimizu, and T. Dunn (1993), Relative depletion of niobium in some arc magmas and the continental crust: Partitioning of K, Nb, La and Ce during melt/rock reaction in the upper mantle, *Earth Planet. Sci. Lett.*, *120*, 111–134, doi:10.1016/0012-821X(93)90234-Z.

Kelemen, P. B., G. M. Yogodzinski, and D. W. Scholl (2003), Alongstrike variation in lavas of the Aleutian island arc: Implications for the genesis of high Mg# andesite and the continental crust, in *Inside the Subduction Factory*, *Geophys. Monogr. Ser.*, vol. 138, edited by J. Eiler, pp. 223–276, AGU, Washington, D. C.

Kessel, R., M. W. Schmidt, P. Ulmber, and T. Pettke (2005), Trace element signature of subduction-zone fluids, melts and supercritical liquids at 120–180 km depth, *Nature*, *437*, 724–727, doi:10.1038/nature03971.

Klemme, S., J. D. Blundy, and B. J. Wood (2002), Experimental constraints on major and trace element partitioning during partial melting of eclogite, *Geochim. Cosmochim. Acta*, *66*, 3109–3123, doi:10.1016/S0016-7037(02)00859-1.

Kurz, M. D., and D. J. Geist (1999), Dynamics of the Galapagos hotspot from helium isotope geochemistry, *Geochim. Cosmochim. Acta*, *63*, 4139–4156, doi:10.1016/S0016-7037(99)00314-2.

Kurz, M. D., W. J. Jenkins, and S. R. Hart (1982), Helium isotopic systematics of oceanic islands and mantle heterogeneity, *Nature*, *297*, 43–47, doi:10.1038/297043a0.

Kurz, M. D., W. J. Jenkins, S. R. Hart, and D. Clague (1983), Helium isotopic variations in volcanic rocks from Loihi Seamount and the Island of Hawaii, *Earth Planet. Sci. Lett.*, *66*, 388–406, doi:10.1016/0012-821X(83)90154-1.

Kurz, M. D., P. S. Meyer, and H. Sigurdsson (1985), Helium isotopic systematics within the neovolcanic zones of Iceland, *Earth Planet. Sci. Lett.*, *74*, 291–305, doi:10.1016/S0012-821X(85)80001-7.

Macpherson, C. G., D. R. Hilton, J. M. D. Day, D. Lowry, and K. Grönvold (2005), High-$^3He/^4He$, depleted mantle and low $\delta^{18}O$, recycled oceanic lithosphere in the source of central Iceland magmatism, *Earth Planet. Sci. Lett.*, *233*, 411–427, doi:10.1016/j.epsl.2005.02.037.

Martin, C. E. (1991), Osmium isotopic characteristics of mantle-derived rocks, *Geochim. Cosmochim. Acta*, *55*, 1421–1434, doi:10.1016/0016-7037(91)90318-Y.

McDonough, W. F. (1991), Partial melting of subducted oceanic crust and isolation of its residual eclogitic lithology, *Philos. Trans. R. Soc. London, Ser. A*, *335*, 407–418, doi:10.1098/rsta.1991.0055.

McDonough, W. F., and S. S. Sun (1995), The composition of the Earth, *Chem. Geol.*, *120*, 223–253, doi:10.1016/0009-2541(94)00140-4.

McInnes, B. I., J. S. McBride, N. J. Evans, D. D. Lambert, and A. S. Andrew (1999), Osmium isotope constraints on ore metal recycling in subduction zones, *Science*, *286*, 512–516, doi:10.1126/science.286.5439.512.

Meisel, T., R. J. Walker, A. J. Irving, and J. P. Lorand (2001), Osmium isotopic compositions of mantle xenoliths: A global perspective, *Geochim. Cosmochim. Acta*, *65*, 1311–1323, doi:10.1016/S0016-7037(00)00566-4.

Moreira, M., and M. D. Kurz (2001), Subducted oceanic lithosphere and the origin of the 'high μ' basalt helium isotopic signature, *Earth Planet. Sci. Lett.*, *189*, 49–57, doi:10.1016/S0012-821X(01)00340-5.

Moreira, M., J. Kunz, and C. J. Allègre (1998), Rare gas systematics in popping rock: Isotopic and elemental compositions in the upper mantle, *Science*, *279*, 1178–1181, doi:10.1126/science.279.5354.1178.

Moreira, M., J. Blusztajn, J. Curtice, S. Hart, H. Dick, and M. D. Kurz (2003), He and Ne isotopes in oceanic crust: Implications for noble gas recycling in the mantle, *Earth Planet. Sci. Lett.*, *216*, 635–643, doi:10.1016/S0012-821X(03)00554-5.

Münker, C., J. A. Pfänder, S. Weyer, A. Büchl, T. Kleine, and K. Mezger (2003), Evolution of planetary cores and the Earth-Moon system from Nb/Ta systematics, *Science*, *301*, 84–87, doi:10.1126/science.1084662.

Niemann, H. B., et al. (1996), The Galileo probe mass spectrometer: Composition of Jupiter's atmosphere, *Science*, *272*, 846–849, doi:10.1126/science.272.5263.846.

O'Nions, R. K., N. M. Evensen, and P. J. Hamilton (1979), Geochemical modeling of mantle differentiation and crustal

growth, *J. Geophys. Res.*, *84*, 6091–6101, doi:10.1029/JB084iB11p06091.

Parman, S. W., M. D. Kurz, S. R. Hart, and T. L. Grove (2005), Helium solubility in olivine and implications for high ^{3}He/^{4}He in ocean island basalts, *Nature*, *437*, 1140–1143, doi:10.1038/nature04215.

Peucker-Ehrenbrink, B., W. Bach, S. R. Hart, J. S. Blusztajn, and T. Abbruzzese (2003), Rhenium-osmium isotope systematics and platinum group element concentrations in oceanic crust from DSDP/ODP Sites 504 and 417/418, *Geochem. Geophys. Geosyst.*, *4*(7), 8911, doi:10.1029/2002GC000414.

Reisberg, L. C., C. J. Allègre, and J. M. Luck (1991), The Re-Os systematics of the Ronda Ultramafic Complex of southern Spain, *Earth Planet. Sci. Lett.*, *105*, 196–213, doi:10.1016/0012-821X(91)90131-Z.

Reisberg, L., A. Zindler, F. Marcantonio, W. White, D. Wyman, and B. Weaver (1993), Os isotope systematics in ocean island basalts, *Earth Planet. Sci. Lett.*, *120*, 149–167, doi:10.1016/0012-821X(93)90236-3.

Righter, K., and E. H. Hauri (1998), Compatibility of Rhenium in garnet during mantle melting and magma genesis, *Science*, *280*, 1737–1741, doi:10.1126/science.280.5370.1737.

Rudnick, R. L. and S. Gao (2003), Composition of the continental crust, in *Treatise on Geochemistry*, vol. 3, *The Crust*, edited by R. L. Rudnick, pp. 1–64, Pergamon, New York.

Rudnick, R. L., M. Barth, I. Horn, and W. F. McDonough (2000), Rutile-bearing refractory eclogites: The missing link between continents and depleted mantle, *Science*, *287*, 278–281, doi:10.1126/science.287.5451.278.

Ryerson, F. J., and E. B. Watson (1987), Rutile saturation in magmas: Implications for Ti-Nb-Ta depletion in island-arc basalts, *Earth Planet. Sci. Lett.*, *86*, 225–239, doi:10.1016/0012-821X(87)90223-8.

Saal, A. E., E. H. Hauri, C. H. Langmuir, and M. R. Perfit (2002), Vapour undersaturation in primitive mid-ocean-ridge basalt and the volatile content of Earth's upper mantle, *Nature*, *419*, 451–455, doi:10.1038/nature01073.

Saal, A. E., M. D. Kurz, S. R. Hart, J. S. Blusztajn, J. Blichert-Toft, Y. Liang, and D. J. Geist (2007), The role of lithospheric gabbros on the composition of Galapagos lavas, *Earth Planet. Sci. Lett.*, *257*, 391–406, doi:10.1016/j.epsl.2007.02.040.

Schmidt, M. W., A. Dardon, G. Chazot, and R. Vannucci (2004), The dependence of Nb and Ta rutile-melt partitioning on melt composition and Nb/Ta fractionation during subduction processes, *Earth Planet. Sci. Lett.*, *226*, 415–432, doi:10.1016/j.epsl.2004.08.010.

Skovgaard, A. C., M. Storey, J. Baker, J. Blusztajn, and S. R. Hart (2001), Osmium-oxygen isotopic evidence for a recycled and strongly depleted component in the Icelandic mantle plume, *Earth Planet. Sci. Lett.*, *194*, 259–275, doi:10.1016/S0012-821X(01)00549-0.

Snow, J. E., and L. Reisberg (1995), Os isotopic systematics of the MORB mantle: Results from altered abyssal peridotites, *Earth Planet. Sci. Lett.*, *133*, 411–421, doi:10.1016/0012-821X(95)00099-X.

Sobolev, A. V., et al. (2007), The amount of recycled crust in sources of mantle-derived melts, *Science*, *316*, 412–417, doi:10.1126/science. 1138113.

Stalder, R., S. F. Foley, G. P. Brey, and I. Horn (1998), Mineral-aqueous fluid partitioning of trace elements at 900–1200°C and 3.0–5.7 GPa: New experimental data for garnet, clinopyroxene, and rutile and implications for mantle metasomatism, *Geochim. Cosmochim. Acta*, *62*, 1781–1801, doi:10.1016/S0016-7037(98)00101-X.

Standish, J. J., S. R. Hart, J. Blusztajn, H. J. B. Dick, and K. L. Lee (2002), Abyssal peridotite osmium isotopic compositions from Cr-spinel, *Geochem. Geophys. Geosyst.*, *3*(1), 1004, doi:10.1029/2001GC000161.

Staudacher, T., and C. J. Allègre (1988), Recycling of oceanic crust and sediments: The noble gas subduction barrier, *Earth Planet. Sci. Lett.*, *89*, 173–183, doi:10.1016/0012-821X(88)90170-7.

Staudigel, H., A. Zindler, A. R. Hart, T. Leslie, C.-Y. Chen, and D. Clague (1984), The isotopic systematics of a juvenile intraplate volcano: Pb, Nd and Sr isotope ratios of basalts from Loihi Seamount, *Hawaii, Earth Planet. Sci. Lett.*, *69*, 13–29, doi:10.1016/0012-821X(84)90071-2.

Stuart, F. M., S. Lass-Evans, J. G. Fitton, and R. M. Ellam (2003), High ^{3}He/^{4}He ratios in picritic basalts from Baffin Island and the role of a mixed reservoir in mantle plumes, *Nature*, *424*, 57–59, doi:10.1038/nature01711.

Sun, S.-S. and W. F. McDonough (1989), Chemical and isotopic systematics of oceanic basalts: implications for mantle composition and processes, in *Magmatism in the Ocean Basins*, edited by A. D. Saunders and M. J. Norry, *Spec. Publ. Geol. Soc.*, *42*, 313–345.

Tolstikhin, I., and A. W. Hofmann (2005), Early crust on top of the Earth's core, *Phys Earth Planet Inter*, *148*, 109–130, doi:10.1016/j.pepi.2004.05.011.

Trull, T. W., and M. D. Kurz (1993), Experimental measurements of ^{3}He and ^{4}He mobility in olivine and clinopyroxene at magmatic temperatures, *Geochim. Cosmochim. Acta*, *57*, 1313–1324, doi:10.1016/0016-7037(93)90068-8.

Wade, J., and B. J. Wood (2001), The Earth's 'missing' Nb may be in the core?, *Nature*, *409*, 75–78, doi:10.1038/35051064.

Walker, R. J., R. W. Carlson, S. B. Shirey, and F. R. Boyd (1989), Os, Sr, Nd and Pb isotope systematics of southern African peridotite xenoliths: implications for the chemical evolution of subcontinental mantle, *Geochim. Cosmochim. Acta*, *53*, 1583–1595, doi:10.1016/0016-7037(89)90240-8.

Weaver, B. L. (1991), The origin of ocean island basalt end-member compositions: Trace element and isotopic constraints, *Earth Planet. Sci. Lett.*, *104*, 381–397, doi:10.1016/0012-821X(91)90217-6.

Weaver, B. L., D. A. Wood, J. Tarney, and J. L. Joron (1987), Geochemistry of oceanic island basalts from the South Atlantic: Ascension, Bouvet, St Helena, Gough and Tristan da Cunha, in *Alkaline Igneous Rocks*, edited by J. G. Fitton and B. G. J. Upton, *Geol. Soc. Spec. Publ.*, *29*, 253–267.

Workman, R. K., and S. R. Hart (2005), Major and trace element composition of the depleted MORB mantle (DMM), *Earth Planet. Sci. Lett.*, *231*, 53–72, doi:10.1016/j.epsl.2004.12.005.

Workman, R. K., S. R. Hart, M. G. Jackson, M. Regelous, K. A. Farley, J. Blusztajn, M. Kurz, and H. Staudigel (2004), Recycled metasomatized lithosphere as the origin of the Enriched Mantle II (EM2) end-member: Evidence form the Samoan Volcanic Chain, *Geochem. Geophys. Geosyst.*, *5*, Q04008, doi:10.1029/2003GC000623.

Zack, T., and T. John (2007), An evaluation of reactive fluid flow and trace element mobility in subducting slabs, *Chem. Geol.*, *239*, 199–216, doi:10.1016/j.chemgeo.2006.10.020.

Zindler, A., and S. R. Hart (1986), Chemical geodynamics, *Annu. Rev. Earth Planet. Sci.*, *14*, 493–571, doi:10.1146/annurev.ea.14.050186.002425.